

**BST-BASED LOW TEMPERATURE  
CO-FIRED CERAMIC (LTCC)  
MODULES FOR MICROWAVE  
TUNABLE COMPONENTS**

**TAO  
HU**

Department of Electrical and  
Information Engineering and  
Infotech Oulu,  
University of Oulu

OULU 2004





*TAO HU*

**BST-BASED LOW TEMPERATURE  
CO-FIRED CERAMIC (LTCC)  
MODULES FOR MICROWAVE  
TUNABLE COMPONENTS**

Academic Dissertation to be presented with the assent of the Faculty of Technology, University of Oulu, for public discussion in Raahensali (Auditorium L10), Linnanmaa, on March 26th, 2004, at 12 noon.

OULUN YLIOPISTO, OULU 2004

Copyright © 2004  
University of Oulu, 2004

Supervised by  
Professor Seppo Leppävuori

Reviewed by  
Professor Marija Kosec  
Doctor Anthony J. Moulson

ISBN 951-42-7291-9 (nid.)  
ISBN 951-42-7292-7 (PDF) <http://herkules.oulu.fi/isbn9514272927/>  
ISSN 0355-3213 <http://herkules.oulu.fi/issn03553213/>

OULU UNIVERSITY PRESS  
OULU 2004

# Hu, Tao, BST-based low temperature co-fired ceramic (LTCC) modules for microwave tunable components

Department of Electrical and Information Engineering and Infotech Oulu, University of Oulu, P.O.Box 4500, FIN-90014 University of Oulu, Finland

2004

Oulu, Finland

## *Abstract*

The recent trend in low temperature co-fired ceramic (LTCC) technology is to integrate more elements into multilayer modules. This thesis describes work specifically aimed at developing ferroelectric barium strontium titanate (BST) for integration into such modules. In particular, an objective was the development of a novel, electric field controlled, tunable component to be used at microwave frequencies (2-26 GHz).

For the application envisaged, relative permittivity is required to be low (100-1000) and adjustable by a suitable applied electric field, the dissipation factor at room temperature must be low ( $\sim 0.001$ ) at 2-26 GHz, and most importantly, the sintering temperature must be suited to the LTCC technology ( $\sim 900$  °C)

Initial work was focused on sol-gel derived  $\text{Ba}_{0.7}\text{Sr}_{0.3}\text{TiO}_3$  powders with boron oxide addition, which were sintered at 900 °C, the dissipation factor was 0.006. The dissipation factor was not low enough for the desired microwave application, and attention turned to powders prepared by the mixed-oxide route. The  $\text{Ba}_{0.7}\text{Sr}_{0.3}\text{TiO}_3$  powders, fluxed with the optimum amounts of boron oxide and lithium carbonate, could be sintered at 890 °C to the same density as is achieved with un-fluxed  $\text{Ba}_{0.7}\text{Sr}_{0.3}\text{TiO}_3$  sintered at 1360 °C. The dissipation factor for this fluxed powder was acceptably low, although permittivity was too high for the particular objective. Subsequently, research was on BST modified by magnesia,  $0.4\text{Ba}_{0.55}\text{Sr}_{0.45}\text{TiO}_3\text{-}0.6\text{MgO}$  (BSTM). With the optimum fluxing additives, the sintering temperature necessary to achieve a dense BSTM-based ceramic was reduced to 950 °C. The developed microstructure was good, and the relative permittivity and dissipation factor values (221, 0.0012 at 1 kHz) at room temperature indicated good microwave properties.

Studies were also undertaken with organic-based tape-casting slurries, laminating procedures and burn-out and sintering schedules. Several kinds of tapes were fabricated and characterized.

A test structure for the measurement of dielectric properties at 26 GHz of the optimized BSTM-based ceramic was constructed. The specimen was 50  $\mu\text{m}$  thick layer of BST on an alumina substrate. The relative permittivity and tunability were 130 and  $>15$  % at  $4 \text{ V } \mu\text{m}^{-1}$  at room temperature. A tunable phase-shifter was fabricated from the same BSTM-based tape using a novel gravure printing technique, and measurements at 26 GHz showed phase shift from 10 to 35° when the electric field was increased from  $1 \text{ V } \mu\text{m}^{-1}$  to  $2.5 \text{ V } \mu\text{m}^{-1}$ .

Some exploratory experiments are described to assess the compatibility of the developed BST-based LTCC with commercial LTCC and some electroceramics.

*Keywords:* BST, LTCC material, microstructure, permittivity, sintering aids, tunability



## Acknowledgements

First of all, I wish to express my deepest gratitude to my supervisor Professor Seppo Leppävuori for his support, advice and guidance and for providing me the opportunity to work at the University of Oulu. I want to express my deep gratitude to Dr. Heli Jantunen for her valuable advice, beneficial discussions and continuous encouragement. I am truly grateful to Dr. Antti Uusimäki for his help and valuable advice.

This research was carried out at the Microelectronics and Materials Physics Laboratories, University of Oulu, Finland, during the years 2001–2003. The work was financially supported by the European project Microwave Electronics with Tunable Dielectric Layers (MELODY, IST-2000-30162), by the EMPART research group of Infotech Oulu, by the Finnish Foundation for Economic and Technology Sciences - KAUTE, and by the Oulun Yliopiston Tukisäätiö.

I want to acknowledge Professor Spartak Gevorgian from Ericsson and all the MELODY members, especially Dr. Anatoli Deleniv for his design and measurement of the components at microwave frequencies. I want to thank everyone in the Microelectronics and Materials Physics Laboratories who have helped me during the work, especially Mr. Timo Vahera, Mr. Marko Kittila, Mr. Jussi Saavalainen and Ms. Johanna Honkamo.

I wish to thank Prof. Marija Kosec and Dr. Anthony J Moulson for their patient reviewing of this thesis. I am truly grateful to Dr. David Iddles for a preview of this thesis and to Ms. Sirkka-Liisa Leinonen for revising the English language of the manuscript.

Finally, I wish to thank my parents and my son for their love, support and encouragement, which gave me the possibility to finish this thesis.

Oulu, January 2004

Hu Tao



## List of symbols and abbreviations

$\epsilon_r$	relative permittivity
$\rho$	bulk density
$\rho_0$	theoretical density
$2\theta$	diffraction angle
$\tan\delta$	dissipation factor
ADS	advanced design system
B98	polyvinyl butyral
BE	back scattering electron mode in SEM
BET	Brunauer-Emmett-Teller, method to measure the specific surface area
BST	barium strontium titanate
BST-o	barium strontium titanate made by mixed-oxide method
BST-sg	barium strontium titanate made by sol-gel technique
BSTB	barium strontium titanate with boron oxide
BSTM	barium strontium titanate with magnesia
BSTM-B	BSTM added with boron oxide
BSTM-L	BSTM added with lithium carbonate
BSTM-BL	BSTM added with boron oxide and lithium carbonate
C	capacitance
CS	coplanar strip
CTE	coefficient of thermal expansion
CVD	chemical vapour-phase deposition
DC	direct current
DTA	differential thermal analysis
$E$	applied bias electric field
EDS	energy dispersive spectroscopy
GRD	ground level
GS	ground-signal probe type
h	thickness of the film
I	electric current
ICP	inductively coupled plasma
JCPDS	joint committee of powder diffraction standards

$K$	commutation quality factor
$L$	length
LS	liquid phase sintering
LTCC	low temperature co-fired ceramic
MEMS	microelectromechanical system
MLMs	multilayer modules
MLCCs	multilayered ceramic capacitors
MOCVD	metallorganic chemical vapour decomposition
$n$	tunability
$n_r$	relative tunability
NZF	ferrimagnetic material $\text{Ni}_{0.55}\text{Zn}_{0.5}\text{Fe}_{1.85}\text{O}_x$
PCB	printed circuit board
PEG	polyethylene glycol
POW	power level
PVA	polyvinyl alcohol
PZT	lead zirconate titanate
$R_{\text{lim}}$	limiting resistor
RA	arithmetic average surface roughness
RF	radio frequency
$s$	line space
SAM	scanning acoustic microscopy
SE	secondary electron mode in SEM
SEM	scanning electron microscopy
SSA	specific surface area
SG	signal-ground probe type
SIG	signal level
S160	butyl benzyl phthalate
$T_c$	Curie temperature
$T_s$	sintering temperature
TEM	transmission electron microscopy
TGA	thermo-gravimetric analysis
XRD	X-ray diffraction
Ucon	polyalkylene glycol
VNA	vector network analyser
$w$	width of the silver line
ZSB	$\text{MgTiO}_3\text{-CaTiO}_3\text{-ZnO-SiO}_2\text{-B}_2\text{O}_3$

## List of original papers

The thesis consists of the compendium and the following six papers, which will be referred to in the text by their Roman numerals.

- I Hu T, Jantunen H, Uusimäki A & Leppävuori S (2003)  $\text{Ba}_{0.7}\text{Sr}_{0.3}\text{TiO}_3$  Powders with  $\text{B}_2\text{O}_3$  additive prepared by the sol-gel method for use as microwave material. *Mater Sci in Semiconductor Processing*, 5: 215-221.\*
- II Hu T, Jantunen H, Uusimäki A & Leppävuori S (2004) BST powder with sol-gel process in tape casting and firing. *J Eur Ceram Soc*, 24: 1111-1116.\*
- III Jantunen H, Hu T, Uusimäki A & Leppävuori S (2004) Tape casting of ferroelectric, dielectric, piezoelectric and ferromagnetic materials. *J Eur Ceram Soc*, 24: 1077-1081.\*
- IV Hu T, Jantunen H, Leppävuori S, Deleniv A & Gevorgian S (2004) Electric-field-controlled permittivity ferroelectric composition for microwave LTCC modules. *J Am Ceram Soc*, 87[4], in press.
- V Deleniv A, Hu T, Jantunen H, Leppävuori S & Gevorgian S (2003) Tunable Ferroelectric Components in LTCC Technology. *IEEE MTT-S Int Microwave Symp Dig*, 3: 1997-2000.†
- VI Jantunen H, Hu T, Uusimäki A & Leppävuori S. Ferroelectric LTCC for multilayer devices. Accepted for the *J Ceram Soc Jap*.

In Paper I,  $\text{Ba}_{0.7}\text{Sr}_{0.3}\text{TiO}_3$  powders with boron oxide ( $\text{B}_2\text{O}_3$ ) addition were prepared by a sol-gel process (BSTB-sg). Ultrafine powders with high specific surface area were obtained, and the sintering temperature of BSTB-sg was reduced to 900 °C.

---

\* Reprinted, with permission from Elsevier Ltd.

† ©2000 EEE. Reprinted, with permission

Papers II and III introduce the tape casting process and the major factors affecting the properties of the tape. BST powders made by sol-gel were used to make tape by adjusting slurry composition (Paper II). Four different powders, including dielectric, ferroelectric, ferrimagnetic and piezoelectric materials, were used to make tapes, and their compatibility for co-firing was tested.

The LTCC composition based on  $0.4\text{Ba}_{0.55}\text{Sr}_{0.45}\text{TiO}_3\text{-}0.6\text{MgO}$  powder was investigated and presented in paper IV. The sintering temperature was decreased from 1400 °C to 950 °C with sintering aids. The microwave devices were fabricated and the results of high-frequency measurements are presented in paper V, which show that the LTCC composition had tunability of >15 % and permittivity of 130 at 26 GHz\*.

Paper VI describes the studies of sintering aids for  $\text{Ba}_{0.7}\text{Sr}_{0.3}\text{TiO}_3$  powders. With a suitable amount of sintering aids, the density of  $\text{Ba}_{0.7}\text{Sr}_{0.3}\text{TiO}_3$  with added  $\text{B}_2\text{O}_3$  and lithium carbonate ( $\text{Li}_2\text{CO}_3$ ) sintered at 890 °C was the same as that of pure  $\text{Ba}_{0.7}\text{Sr}_{0.3}\text{TiO}_3$  sintered at 1360 °C. The BST tapes were also laminated and co-fired with commercial dielectric LTCC, which demonstrates the potential for the integration of a tunable BST component within a LTCC multilayer unit.

The work presented here was carried out in the Microelectronics and Materials Physics Laboratories, University of Oulu, Finland. The experimental work described in the papers I–VI was the contribution of the author. The analyses and measurements of dielectric properties at low frequencies were carried out by the author, whereas the high-frequencies measurements and component design were performed in Chalmers University of Technology, Gothenburg, Sweden. The papers I–IV were written by the author with the kind help of the co-authors. In Paper V, the fabrication of the component was the contribution of the author, and in Paper VI, the author contributed the basic idea and carried out the experimental work.

---

\* Unless specifically stated otherwise, the term ‘permittivity’ is used throughout the thesis instead of the correct ‘relative permittivity’. This is done for the sake of brevity and is in accordance with common usage.

# Contents

Abstract	
Acknowledgements	
List of symbols and abbreviations	
List of original papers	
Contents	
1 Introduction .....	13
1.1 Tunable BST material in LTCC modules for microwave devices .....	13
1.2 Objective and outline of the thesis .....	16
2 Fundamentals of BST in a LTCC module .....	17
2.1 BST materials for tunable devices .....	17
2.2 Powders and sintering .....	19
2.3 Tape casting process .....	21
2.4 LTCC technology .....	23
3 Experimental procedures .....	25
3.1 Powder and ceramic preparation .....	25
3.1.1 The sol-gel route .....	25
3.1.2 The mixed-oxide route .....	26
3.2 Fabrication of tapes and components .....	26
3.3 Materials characterization .....	27
4 Results and discussions .....	29
4.1 LTCC powders based on BST .....	29
4.1.1 BST and BSTB powders prepared by the sol-gel method .....	29
4.1.2 BST with sintering aids of $B_2O_3$ and $Li_2CO_3$ .....	31
4.1.3 BSTM with sintering aids of $B_2O_3$ and $Li_2CO_3$ .....	34
4.2 Fabrication of tapes and laminates .....	37
4.3 Microwave measurements .....	39
4.3.1 Microwave characterization .....	39
4.3.2 Phase-shifter .....	41
4.4 Co-firing of BST-BL tape with other tapes .....	43
5 Conclusion .....	46
References .....	48



# 1 Introduction

## 1.1 Tunable BST material in LTCC modules for microwave devices

Barium strontium titanate (BST) is one of the most important ferroelectric materials widely used in many applications. BST has been studied for application in microwave devices since the early 1960s (Rupprecht & Bell 1962). It is well known that BSTs are of high permittivity, high tunability and compatibility with high-temperature superconductors (Lancaster *et al.* 1998). Because of their tunability, or change in permittivity as a function of the electric field, BST materials have been intensively investigated for microwave applications (Tombak *et al.* 2000, Babbitt *et al.* 1995, Zimmermann *et al.* 2001). Recently, research on tunable microwave BST materials in LTCC modules for miniaturization has become a topic of interest for many researchers and engineers working in the field of materials science and microelectronics.

Application of tunable components based on BST with a LTCC module provides a route to more integrated, miniaturized and reconfigurable microwave systems. The dependence of permittivity on electric fields makes it possible to develop a wide range of devices with enhanced functionality and performance. It is well known that ferroelectrics have two states: the ferroelectric state below  $T_c$  (polar phase) and the paraelectric state above  $T_c$  (non-polar phase), as shown in Fig. 1. Ferroelectrics especially in the paraelectric state are regarded as attractive materials for applications in electrically tunable microwave devices, due to several reasons including losses and hysteresis (Gevorgian & Kollberg 2001). The transition temperature of BST from ferroelectric to paraelectric state, or the Curie temperature ( $T_c$ ), varies as a function of the Ba/Sr ratio (Syamaprasad *et al.* 1988). The adjustment of the Ba/Sr ratio makes BST material available to be used in the non-polar phase at different ambient temperatures. In the present study,  $\text{Ba}_{0.7}\text{Sr}_{0.3}\text{TiO}_3$ ,  $\text{Ba}_{0.55}\text{Sr}_{0.45}\text{TiO}_3$  and  $0.4\text{Ba}_{0.55}\text{Sr}_{0.45}\text{TiO}_3-0.6\text{MgO}$  were used as the basic BST materials. They are typical ferroelectric materials with  $T_c$  310 K, 254 K and 209 K, respectively, and MgO is an effective additive that decreases permittivity and the dissipation factor as well (Sengupta *et al.* 1995).

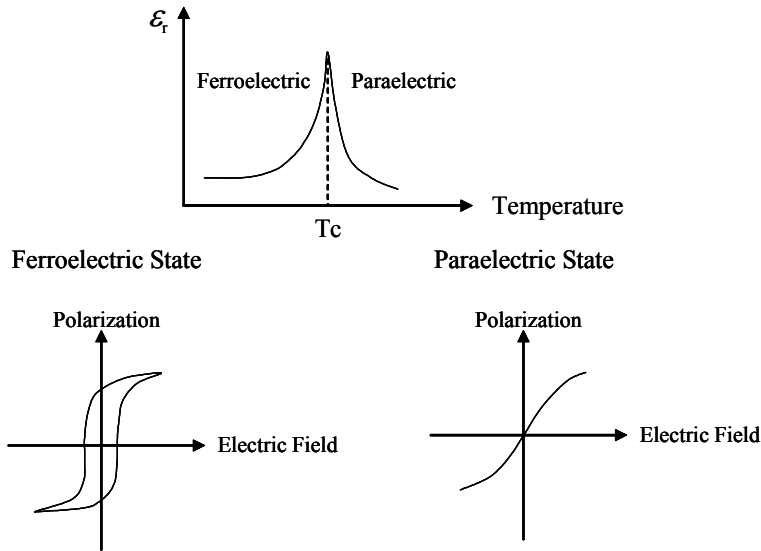


**Fig. 1. Temperature dependence of ferroelectric behaviour.**

The relative permittivity of ferroelectrics varies with the applied electric field, resulting in, for example, a change of phase velocity in the microwave device, which allows tuning in real time for a particular application. Different microwave devices have been developed based on this valuable property. Examples of the applications of ferroelectric BST films include tunable resonators, filters (Tombak *et al.* 2001, Baily *et al.* 1997) and phase-shifters (Zimmermann *et al.* 2001, De Flaviis *et al.* 1997, Acikel *et al.* 2001), variable-power dividers and variable-frequency oscillators. Such components have a wide range of application in telecommunication and radar systems for both military and commercial services. Nowadays, there are some products available, such as tunable filters, diplexers, delay lines and oscillators made by Paratek Microwave Inc. ([www.paratek.com](http://www.paratek.com)).

BST thin films are commonly prepared by physical vapour deposition (PVD) (sputtering, pulsed laser deposition) (Padmini *et al.* 1999, Outzourhit *et al.* 1995, Miranda *et al.* 1995), metallorganic chemical vapour decomposition (MOCVD) (Ayuavives *et al.* 2000) and the sol-gel method with spin coating (Jang & Jang 1998, De Flaviis *et al.* 1996). These methods are difficult and expensive to execute in industrial production because of the need for high vacuum, with exception of the sol-gel method, and all require high-quality supporting substrates for the BST films. Screen printing is also used to produce BST thick films sintered at high temperature (1100 °C) (Su & Button 2001, Zimmermann *et al.* 2001).

Recently, a tape casting process exploiting the LTCC technique was developed as a cost-effective and efficient method for producing multilayer modules (MLMs) not only for microwave applications but also for automobile and consumer electronic applications. LTCC technology consists in slurry preparation and tape casting, followed by punching

vias, the metal patterning of a single layer and stacking of the multilayer structure, followed by lamination and co-firing (Jantunen 2001).

Manufacturing of BST tunable films with the LTCC technique is an attractive challenge. The first key question to be solved is the sintering temperature ( $T_s$ ) of BST, which is too high for using silver electrodes and co-firing with LTCC multilayer modules (850–900 °C). Pure BST and BST-based materials are commonly sintered at >1350 °C (Zimmermann *et al.* 2001, Erker *et al.* 2000, De Flaviis *et al.* 1997), which is why platinum or refractory metals are used as inner conductors. Platinum electrodes are expensive, and their electrical performance is relatively poor, which is why cost-effective fabrication of high-quality components is difficult. Reduction of the sintering temperature of BST to around 900 °C would enable the use of cheaper and highly conductive silver as the inner conductor. Furthermore, this novel technology would allow true integration of such BST components with dielectric LTCC structures. Another important issue is the compatibility of BST tape with dielectric LTCC tapes. Slurry compositions should be adjusted to make good tapes with proper shrinkage and tensile strength. The shrinkage and adhesion of different tapes and the diffusion problems should be studied carefully to achieve real integration of the multilayer structure. A possible future LTCC integrated device is shown schematically in Fig. 2. Integration of ferroelectric layers into multilayer ceramic modules including dielectric layers, piezoelectric layers, ferrimagnetic layers and passive components with all layers prepared by tape casting would enable miniaturization and inexpensive mass production.

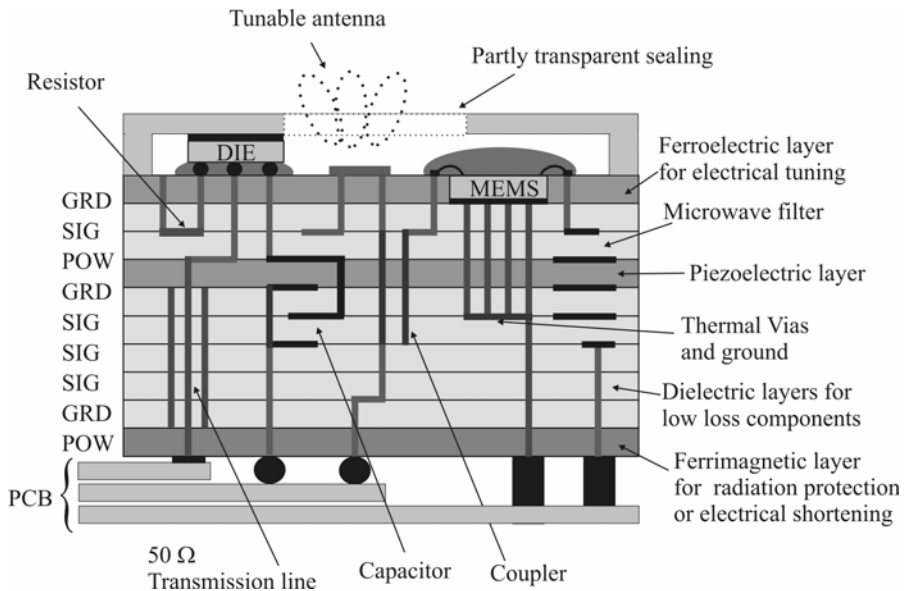


Fig. 2. The cross-section of a future LTCC structure (Hu *et al.* 2003).

## 1.2 Objective and outline of the thesis

The principal objective of the research described in this thesis is to develop tunable BST components for LTCC technology with good performance at microwave frequencies. At first, ultrafine powders together with the sintering aids are investigated to decrease the high sintering temperature of BST materials with minimum influence on the dielectric properties. The sol-gel process is studied for making ultrafine BST powder and  $B_2O_3$ -added powders (BSTB). The properties of the powders and the bulk ceramics of BST and BSTB are characterized. Then the sintering aids  $Li_2CO_3$  and  $B_2O_3$  are investigated for different BST powders prepared by the mixed-oxide method. Sintering behaviour, microstructure and dielectric properties at low frequencies are studied. Secondly, the tape casting process is studied to make good tapes by using these low sintering temperature BST-based compositions. The slurry composition and the process parameters are optimized, and the tapes are characterized. Thirdly, a basic test structure and a tunable phase-shifter are fabricated using BST-based LTCC tapes, and microwave properties, such as permittivity and tunability, are measured. Special attention is given to the fabrication, sintering behaviour and microstructure of the BST-based LTCC materials. Co-firing of BST tape with commercial dielectric LTCC tape and other tapes are also studied.

## 2 Fundamentals of BST in a LTCC module

### 2.1 BST materials for tunable devices

BST solid solution belongs to A-position substitution of perovskite barium titanate.  $\text{SrTiO}_3$  ( $T_c \sim -250$  °C) is introduced into the  $\text{BaTiO}_3$  perovskite structure to lower the Curie temperature of  $\text{BaTiO}_3$  ( $\sim 120$  °C) and to modify the dielectric properties. When strontium is added,  $\text{Ba}^{+2}$  ions are partly replaced by  $\text{Sr}^{+2}$  ions. The Curie temperature of  $\text{Ba}_x\text{Sr}_{1-x}\text{TiO}_3$  single crystals decreases linearly with an increase of the  $\text{Sr}^{+2}$  concentration (Moulson & Herbert 2003). As shown in Fig. 3a, the Curie temperature of  $\text{Ba}_x\text{Sr}_{1-x}\text{TiO}_3$  ceramic materials is also reduced by an increasing amount of  $\text{SrTiO}_3$ . Ceramic BST has a higher Curie temperature than single-crystal BST with the same composition, because the grains of a ceramic sample may have differences in stoichiometry, and pores and cavities are typically present (Vendik & Zubko 2000). Furthermore, the addition of strontium also changes permittivity at  $T_c$ . The maximum permittivity of  $\text{Ba}_x\text{Sr}_{1-x}\text{TiO}_3$  first increases and then decreases ( $x < 0.4$ ) along with the increase of  $\text{SrTiO}_3$  (Fig. 3b).

The main attraction of BST materials is the strong dependence of their relative permittivity ( $\epsilon_r$ ) on the applied bias electric field ( $E$ ). This characteristic is commonly described by tunability,  $n$ , defined as the ratio of permittivity with zero applied electric field to that measured with a field,  $E$ , applied,

$$n = \frac{\epsilon_r(0)}{\epsilon_r(E)} \quad (1)$$

Relative tunability ( $n_r$ ) is defined as

$$n_r = \frac{\epsilon_r(0) - \epsilon_r(E)}{\epsilon_r(0)} = 1 - \frac{1}{n} \quad (2)$$

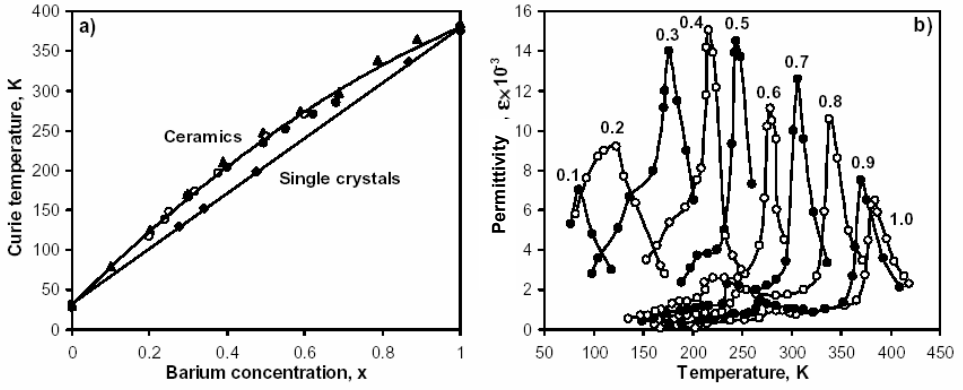


**Fig. 3. (a) Curie temperature of  $\text{Ba}_x\text{Sr}_{1-x}\text{TiO}_3$  ceramic and single-crystal materials as a function of barium concentration  $x$  (Vendik & Zubko 2000), and (b) temperature dependencies of the permittivity values of  $\text{Ba}_x\text{Sr}_{1-x}\text{TiO}_3$  ceramic materials for different barium concentrations (Smolenskii & Isupov 1954).**

For ferroelectric materials, normally, the higher is the relative permittivity, the higher is tunability and the larger the dissipation factor. However, microwave applications require high tunability coupled with a low dissipation factor. Thus, a parameter called the Commutation Quality Factor ( $K$ ) has been introduced to characterize tunable performance and the dissipation factor. The Commutation Quality Factor of ferroelectrics is (Vendik *et al.* 2000)

$$K = \frac{(n-1)^2}{n \cdot \tan \delta(0) \tan \delta(E)} \quad (3)$$

where  $E$  is the electric field applied to the ferroelectric,  $n$  is tunability and  $\tan \delta$  is the dissipation factor.

Tunability of 10–60 % at  $4 \text{ V } \mu\text{m}^{-1}$ , low dissipation factor ( $<0.001$ ) and suitable relative permittivity (100–1000) are commonly required for tunable microwave devices. MgO was introduced into BST material to decrease permittivity and the dissipation factor (Sengupta *et al.* 1995, Su & Button 2004), because the BST material itself has too high permittivity (1000–15500). Fig. 4 shows the effects of variable amounts of MgO on the dielectric property of  $\text{Ba}_{0.8}\text{Sr}_{0.2}\text{TiO}_3$  (Su & Button 2004). Permittivity decreases with increasing amounts of MgO, and the Curie temperature shifts towards lower temperatures. Dissipation factor also decreases with increasing MgO.

At low MgO doping concentrations  $\sim 2$  mol%, Mg acts as an acceptor to replace Ti at the B site of the  $\text{ABO}_3$  perovskite structure, leading to the shift of  $T_c$  towards lower temperatures and a diffused phase transition. The permittivity and the dissipation factor are gradually suppressed as the Mg content increases and the grain size decreases

drastically. At higher MgO doping concentrations  $\sim >2$  mol%, further suppression of permittivity and dissipation factor without any  $T_c$  shift are observed, which indicates a ‘composite’ mixing effect. Grain size remains almost constant. MgO may precipitate out and segregate at grain boundaries, which ‘dilute’ permittivity, hinder abnormal grain growth, and minimize the domain-wall contribution to the dissipation factor (Su & Button 2004).

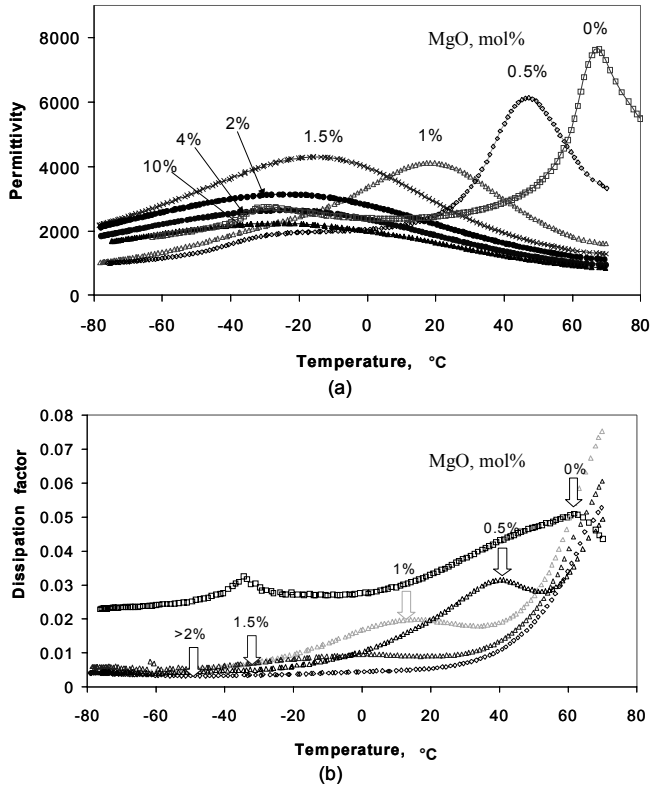


**Fig. 4. (a) Permittivity and (b) dissipation factor (at 10 kHz) of  $\text{Ba}_{0.8}\text{Sr}_{0.2}\text{TiO}_3$  ceramics with different MgO addition (Su & Button 2004).**

## 2.2 Powders and sintering

The microstructure, properties and final performance of ceramic materials are dependent on the nature of the raw material powders. Purity, particle size and its distribution, reactivity, polymorphic form, availability and cost must be considered and carefully controlled. Multi-component powders can be prepared by two techniques: mixed-oxide method (or solid state synthesis) and chemical methods. Ball milling and attrition milling are often used in mixed-oxide method. The sol-gel and aqueous precipitation are common chemical methods.

Sol-gel is a generic term for a variety of techniques used to achieve high-purity composition with homogeneity at the molecular level. Powder preparation with the sol-gel approach involves several steps. First, a stable dispersion (sol) of particles less than 0.1  $\mu\text{m}$  in diameter is formed in a liquid from inorganic or organic precursors. Based on a change in concentration (evaporation of a portion of the liquid), aging, or an addition of a suitable electrolyte, change in the pH value of the liquid, three-dimensional bonding will occur throughout the sol to form a gel. The remaining liquid is evaporated from the gel by heating or freeze-drying. Finally, the ceramic composition is obtained by increasing the temperature to convert the dehydrated gel into a powder (Brinker & Scherer, 1990). The sol-gel process has been used to prepare fine powders, thin films, porous materials, single crystals and monoliths. Powders made by the sol-gel method have high purity, molecular-scale homogeneity, enhanced reactivity (lower processing temperature) and controlled size and shape. The sol-gel process is especially suitable for the fabrication of complex mixture powders with small amounts of additives (Abe *et al.* 1990, Ritter *et al.* 1986).

Sol-gel powders as well as all other powders are characterized by specific surface area (SSA), particle size and distribution. The properties of the powder will determine the properties of the sintered bulk ceramic or film, such as density, microstructure, grain size and electrical properties.

The sintering of ceramics to full density is a very important step in the production procedure and can affect the microstructure and properties of the ceramics (Moulson & Herbert 2003, Kingery *et al.* 1976). Sintering essentially aims to remove the pores between the starting particles (accompanied by shrinkage of the component) and to enable growth together between adjacent particles. Sintering is divided into three stages:

1) Initial stage: rearrangement of particles and initial neck formation at the contact point between each pair of particles. Slight movement or rotation of adjacent particles increase the number of contact points. Bonding occurs at the points of contact, where material transport may occur and surface energy is the highest.

2) Intermediate stage. The size of the necks between particles grows and grain boundaries lengthen. Porosity decreases and particles move closer to each other. Most of the shrinkage occurs during this second stage.

3) Final stage. Porosity is removed by vacancy diffusion along grain boundaries. Pore removal and vacancy diffusion are aided by movement of the grain boundary and controlled grain growth (driven by surface energy). However, if grain growth is too fast, the grain boundaries may move faster than the pores and leave them isolated inside a grain. Therefore, grain growth must be controlled to achieve maximum removal of porosity (Richerson 1992).

Sintering may occur by a variety of mechanisms as summarized in Table 1.

*Table 1. Sintering Mechanisms (Richerson 1992).*

Type of sintering	Material transport mechanism	Driving force
Vapour-phase	Evaporation-condensation	Differences in vapour pressure
Solid-state	Diffusion	Differences in free energy or chemical potential
Liquid-phase	Viscous flow, diffusion	Capillary pressure, surface tension
Reactive liquid	Viscous flow, solution-precipitation	Capillary pressure, surface tension

Liquid phase sintering (LS) is a sintering process in which a liquid phase coexists with a particulate solid at the sintering temperature during at least part of the thermal cycle. This is acceptable in systems where grain boundary impurities (e.g. frozen liquid) are tolerated and the liquid additive resides only temporarily at the grain boundaries during the early stages of LS. The solid must be soluble in the liquid. Liquid-phase sintering enables rapid densification kinetics. It is much faster than solid-state sintering, due to the higher diffusivity and mass transport in liquids. Liquid capillary action (equivalent to high external pressure) aids in the rearrangement of particles in the early stages of sintering. Also, the enhanced reactivity of a liquid with solids results in densification due to a rapid dissolution-transport-precipitation phenomenon. LS is utilized widely for consolidation of both metallic and ceramic powders.

There are several methods to obtain a liquid phase during sintering, mixing of powders with different compositions and melting points, or formation of a eutectic during the processing of ceramic powders. Due to particle repulsion at wetting angles  $>90^\circ$ , a powdered solid cannot be densified with the assistance of a non-wetting liquid. The rate of LS is controlled by particle size, viscosity and wetting angle and is strongly affected by temperature.

An effective way to decrease sintering temperature is to add sintering aids that have low melting points (Wang *et al.* 1994). In general, the sintering aids for ceramics are glasses or glass ceramics that soften at rather low temperatures (Tummala *et al.* 1991). The liquid that forms during sintering promotes densification and grain coarsening at lower temperatures. These phases generally degrade electrical properties. However, it is possible to choose some glass or glass ceramics that have a less degrading effect on the properties. One interesting possibility is to add  $B_2O_3$ , whose melting point is  $450^\circ C$ , as a sintering aid (Ho 1994). For example, Rhim *et al.* were able to decrease the sintering temperature of BST prepared by the conventional mixed-oxide method from  $1350^\circ C$  to  $1150^\circ C$  with 0.5 wt%  $B_2O_3$  (Rhim *et al.* 2000). This  $B_2O_3$ -doped BST sintered at  $1150^\circ C$  had the same dielectric properties as pure BST sintered at  $1350^\circ C$ . Over-doping of BST with  $B_2O_3$  ( $>1.0$  wt%), however, led to the formation of a secondary phase that degraded the dielectric properties of the ceramics.

Other sintering aids, such as  $Y_2O_3$ ,  $Bi_2O_3$ ,  $Nb_2O_5$ , MnO, FeO, LiF,  $SiO_2$ ,  $TiO_2$ , and  $Al_2O_3$ , are also used for BST ceramics by Herner (Herner *et al.* 1993). In present study, the sintering aids were chosen based on the literature and the experimental results on shrinkage behaviour, phase composition and electrical performance.

### 2.3 Tape casting process

Tape casting is a well-known technique in paper and plastic manufacturing. Since Howatt published the first paper (Howatt, 1947) on the casting process developed for ceramic material, tape casting has become a feasible method for preparing ceramic multilayer devices. Nowadays, tape casting is widely used in the electronics industry for multilayered ceramic capacitors, piezoelectric and electrostrictive devices, multilayered ceramic packages, ceramic substrates, fuel cells and catalytic substrates.

The main advantage of the tape casting process is that it enables the production of large, flat ceramic layers typically ranging in thickness from 0.025 mm to 1.27 mm (Mistler & Twiname 2000). Additionally, there are no fundamental restrictions concerning the use of solvent/binder systems, and the process can be set up either as an inexpensive continuous process to manufacture large quantities of smooth tapes or as a small laboratory route for cost-effective testing applications. A ‘green’ tape is formed by spreading a slurry consisting of ceramic powders carried in an organic (or water) vehicle, together with appropriate binder and dispersant. In the present study the layer was formed by doctor-blading. This consists in running the slurry from a reservoir as it moves relative to an appropriate surface. The slurry is spread to a defined thickness determined by the setting of a following doctor blade. The tape casting process is shown in Fig. 5. The characterization of powders is very important for tape casting. SSA, particle size and distribution, trace impurity level and specific gravity should be measured and considered before making the slurry. Generally, most powders fall within a SSA range of 1 to 50 m<sup>2</sup>g<sup>-1</sup>, with the vast majority of highly sinterable powders falling within 5–15 m<sup>2</sup>g<sup>-1</sup> (Mistler & Twiname 2000).

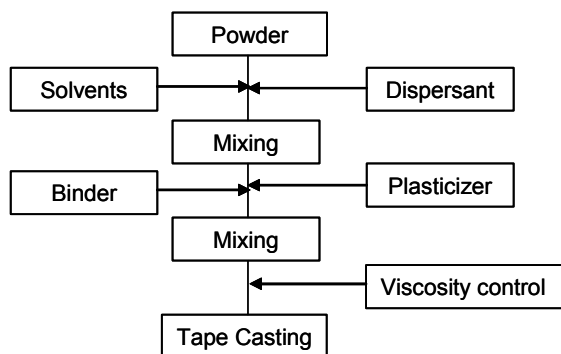


**Fig. 5. Flow chart of the tape casting process (Hu *et al.* 2003).**

In the tape casting process, the important properties of the slurry are influenced by the binder, dispersant, plasticizer and organic vehicle. The dispersant or deflocculant breaks apart the agglomerates into individual particles, wets the particles and maintains a fluid layer between the primary particles by both steric hindrance (physically prohibiting one particle from coming into contact with another particle by putting a coating on it) and ionic repulsion (repelling particles from one another by charging particle surfaces). It is important to produce a well-dispersed, deflocculated, and stabled suspension of the ceramic powders. The binder supplies a network of polymer matrix that holds the entire chemical system together for further processing. The binder has the greatest effect on the green tape properties, such as strength, flexibility, plasticity, laminability, durability, roughness and printability. The following factors must be considered when choosing the binder: solubility, viscosity, cost, strength, glass transition temperature, firing atmosphere of the powder, ash residue, burnout temperature and by-products. The plasticizer makes

the green tape bendable without cracking during the process of punching, cutting, rolling and laminating. The solvent should have good solubility for the binder and plasticizer and a moderate evaporation rate after casting while being environmentally ‘friendly’. Normally, nonaqueous media are used for ceramic powders, and multiple solvents are usually employed to improve the solubility of the binders and plasticizers and to achieve greater control over drying speed. Many organic reagents are available for solvents and additives.

The slurry is characterized by viscosity, specific gravity and zeta potential. For example, slurry viscosity should be carefully controlled because tape thickness decreases with decreasing viscosity. The optimal viscosity values for tape casting slurries were 500 to 25000 mPa s according to Cahn (Cahn *et al.* 1996). The criterion for a good slurry was the potential to cast a thin and uniform tape. This was enabled by Newtonian type viscosity (Joshi *et al.* 2002). Furthermore, high tensile strength and high density of green tape are desirable qualities.

## 2.4 LTCC technology

LTCC is a relatively new processing technology for the packaging of microelectronics (Scrantom & Lawson 1999, Kageyama *et al.* 2001, Ishizaki *et al.* 2000). It is similar to the high-temperature co-fired systems used in fabricating multilayered ceramic packages by high temperature co-firing ceramics (HTCC), with the exception of the low co-firing temperature 850–950 °C. LTCC technology consists of two main processes. First, an appropriate slurry is prepared of ceramic powders and vehicle combined with surfactant, binders, and plasticizers, and then tape casting is done to get a tape and the tape is formed as described above (Fig. 5). Second, the green tapes are shaped and drilled by laser beams or mechanical punching to form vias. After filling the vias with metal paste (e.g. Ag or Au), the tape is positioned and printed with conductive paste to obtain the designed circuits. Then, several layers of differently patterned tapes are positioned and stacked, followed by lamination. Three basic parameters in lamination (temperature, pressure and time) must be controlled. The laminating temperature depends basically on the type and amount of plasticizers and binder in the slurry, and is typically in the range of 70–90 °C (Mistler & Twiname 2000). The dwell time of lamination must be sufficient to heat the entire stack and the number of layers and overall structure should also be considered. Sufficient pressure must be applied to provide intimate contact between the layers without distorting the laminated part (Cahn *et al.* 1998). The final stage is the firing of the laminate. This is a critical stage and must be carefully controlled so as to ensure removal of all organics without disrupting the structure prior to the final sintering temperature being reached, which is typically in the range of 850–900 °C. Fig. 6 illustrates the LTCC process adopted in the Microelectronics and Materials Physics Laboratories, University of Oulu.

The main advantage of the LTCC technology is that it enables the achievement of high component density and the utilization of high-conductivity metals (Ag) in embedded metallization. LTCC technology processes the layers in parallel; each layer can be

inspected separately and mistakes can be corrected before lamination, which results in high reliability and cost-effective production (Barnwell & O'Neill 1997).

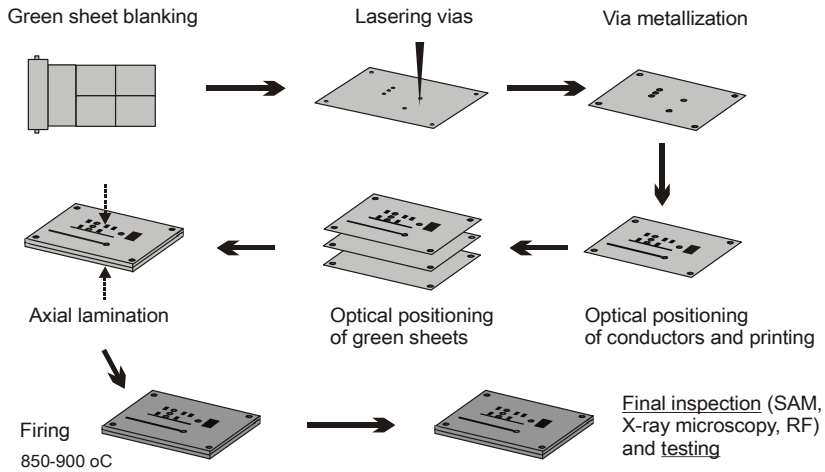


**Fig. 6. Flow chart of the LTCC process.**

An even more important point for microwave applications of BST in LTCC modules is that it has suitable permittivity, a low dissipation factor and high tunability and is cost-effective. The integration of BST LTCC layers with commercial dielectric LTCC layers, including passive components on the dielectric layers and tunable elements on BST layers, results in future LTCC modules as shown in Fig. 2.

## 3 Experimental procedures

### 3.1 Powder and ceramic preparation

#### 3.1.1 The sol-gel route

LTCC powders were prepared first by the sol-gel method. The sol-gel process used is shown in Fig. 7. The starting materials were barium acetate ( $\text{Ba}(\text{CH}_3\text{COO})_2$ , 99.0 %), strontium acetate ( $\text{Sr}(\text{CH}_3\text{COO})_2$ , 99.9 %), titanium isopropoxide ( $\text{Ti}(\text{OCH}(\text{CH}_3)_2)_4$ , 97 %) and boron propoxide ( $\text{B}(\text{OCH}_2\text{CH}_2\text{CH}_3)_3$ , 98 %) purchased from Aldrich Chemical Company.

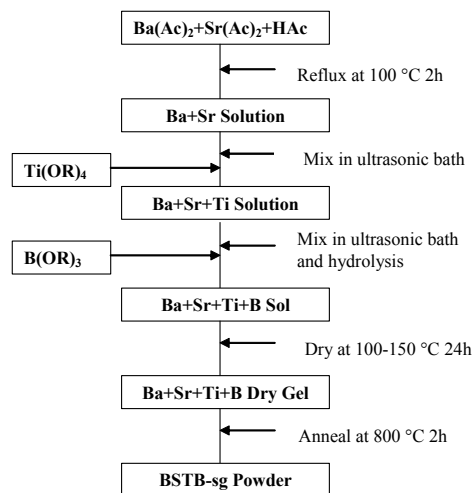


Fig. 7. Flow diagram of the synthesis of BST-based powders by the sol-gel method (Paper I).

Three different powders were prepared 'in-house' by the sol-gel method, and their compositions are given in Table 2 together with their identifying codes. BST-o was  $\text{Ba}_{0.7}\text{Sr}_{0.3}\text{TiO}_3$  powder prepared by the conventional mixed-oxide method supplied by Fuji Titanium Industry Co. Ltd. (Japan).

*Table 2. Method of preparation and compositions of different powders (Paper I).*

	BST-o	BST-sg	BSTB1-sg	BSTB2-sg
method	mixed-oxide	sol-gel	sol-gel	sol-gel
Ba:Sr:Ti	0.70:0.30:1.00	0.70:0.30:1.00	0.78:0.34:1.00	0.85:0.36:1.00
$\text{B}_2\text{O}_3$ / wt%	0	0	4.12	6.08

### **3.1.2 The mixed-oxide route**

Using the mixed-oxide method, basic BST powders ( $T_s > 1350$  °C) were added with additives for sintering at 850–950 °C. The three basic BST powders were:

- 1)  $\text{Ba}_{0.7}\text{Sr}_{0.3}\text{TiO}_3$  powder obtained by Fuji Titanium Industry Co. Ltd. (Japan),
- 2)  $\text{Ba}_{0.55}\text{Sr}_{0.45}\text{TiO}_3$  and  $0.4\text{Ba}_{0.55}\text{Sr}_{0.45}\text{TiO}_3\text{-}0.6\text{MgO}$  powders supplied by the project partner Filtronic Comtek Ltd. (UK).

Based on their data sheets, the SSA and mean particle size of the powders are  $2.43 \text{ m}^2\text{g}^{-1}$  and  $1.00 \mu\text{m}$  for  $\text{Ba}_{0.7}\text{Sr}_{0.3}\text{TiO}_3$ ,  $6.19 \text{ m}^2\text{g}^{-1}$  and  $1.22 \mu\text{m}$  for  $\text{Ba}_{0.55}\text{Sr}_{0.45}\text{TiO}_3$ ,  $7.62 \text{ m}^2\text{g}^{-1}$  and  $0.85 \mu\text{m}$  for  $0.4\text{Ba}_{0.55}\text{Sr}_{0.45}\text{TiO}_3\text{-}0.6\text{MgO}$ , respectively. However, when the components and test structures for microwaves were prepared, only compositions based on  $\text{Ba}_{0.55}\text{Sr}_{0.45}\text{TiO}_3$  and  $0.4\text{Ba}_{0.55}\text{Sr}_{0.45}\text{TiO}_3\text{-}0.6\text{MgO}$  powders were used. The LTCC BST composition was optimized following the experimental results of sintering behaviour, phase composition and electrical properties.

The mixed-oxide route was done by weighing the calculated amounts of the basic powders,  $\text{Li}_2\text{CO}_3$  and  $\text{B}_2\text{O}_3$ , after which they were mixed and ball-milled together with binder (PVA) and plasticizer (PEG).

## **3.2 Fabrication of tapes and components**

The tapes were fabricated using various powders, including pure BST, BSTM, powders with addition of sintering aids and sol-gel powders.

Before making the slurry, the SSA, particle size and distribution of ceramic powders were measured. The slurries were prepared with a ball mill. The powders were added to solvents and dispersants and mixed for 24 hours, after which binder and plasticizers were added to the mixture and mixing was continued for another 24 hours. The solvents were ethanol and xylene, which are commonly used in the tape casting process. Menhaden fish oil, which was used in our experiment, is an effective dispersant that also acts as a surfactant, as it contains glycerol esters of saturated and unsaturated fatty acids. Polyvinyl butyral (B98) was used as binder together with butyl benzyl phthalate (S160) and polyalkylene glycol (Ucon) used as plasticizers. All these organic additives were supplied

by Richard E. Mistler, Inc., Morrisville, USA. The viscosity of the slurry was measured and controlled before casting.

The casting was done by a laboratory caster Unicaster 2000 (University of Leeds, Leeds, UK) with a single doctor blade and 100–400  $\mu\text{m}$  gaps. According to the designed structures of the different components, the tapes were shaped and laminated into multilayer modules, or the tape was laminated on alumina substrates, at 70 °C and 15–20 MPa for 15–20 min and then fired at different temperatures. During the initial part of the firing schedule (200–600 °C) the heating rate was 1 °C  $\text{min}^{-1}$  to safely remove the organics; when this stage was completed the rate was increased by 3 °C  $\text{min}^{-1}$  to the sintering temperature. Screen printing and direct gravure printing were used to produce the silver pattern.

### 3.3 Materials characterization

The dry gel was characterized by thermo-gravimetric analysis (TGA) and differential thermal analysis (DTA). Simultaneous measurements were executed in air by a thermal analyzer (NETZSCH STA-409 EP, Selb/Bayern, Germany).

The specific surface areas (SSA) of the powders were measured by a BET analyzer COULTER OMNISORP 360CX (Coulter Electronics Inc. Ltd. Luton, UK). The particle size distribution was measured by Malvern Mastersizer (MS1002, Malvern Instruments Ltd., Malvern, UK).

A binder (2 wt% PVA) and a plasticizer (0.7 wt% PEG) were added to the powders, which were then die-pressed into cylindrical pellets 18–25 mm in length and 10–12 mm in diameter for dilatometric measurements (Orton Automatic Recording Dilatometer, Westerville, OH, USA). The results were used to determine the sintering temperature of the bulk sample.

The crystal phase composition was studied by X-ray diffraction (XRD, Siemens D5000, Karlsruhe, Germany) utilizing the JCPDS data file (International Center for Diffraction Data 1992, Swarthmore, PA, USA).

The quantitative chemical analyses of the BST-based ceramic samples were made using a PU7000 ICP spectrometer (Philips, Netherlands) and energy dispersive spectroscopy (EDS). The microstructures were revealed by scanning electron microscopy (SEM, Jeol JSM-6400, Tokyo, Japan).

The viscosities of the slurries at room temperature were measured using a Brookfield digital viscometer DV-II+ Version 2.0 (with spindle SC4-18) (Brookfield engineering laboratories, INC., Stoughton, USA). The surface roughness (RA) and tensile strength of the cast and dried ‘green’ tapes were measured by Dektak3ST (Sloan Technology, Santa Barbara, CA, USA) and Instron 8801 tensile strength testers (Instron Company, UK), respectively.

The microstructures of the ‘green’, laminated and fired tapes were revealed by SEM. Shrinkage and mass loss were estimated from the dimensions and weights of the laminated ‘green’ and fired tapes.

For electrical measurements of the ceramic bulk at low frequencies 1 kHz–1 MHz, cylindrical samples with a diameter of 12.5 mm and thickness ranging from 1.5 to 2 mm

were pressed and sintered. The heating rate for each firing was chosen as  $3\text{ }^{\circ}\text{C min}^{-1}$ , which has been reported to be slow enough to produce high-density ceramics with small phase transition broadening (Rhim *et al.* 2000). Dwell time at the sintering temperature was 1 hour. The end surface electrodes were prepared using conductive silver paste Heraeus DT1402. Permittivity and dissipation factor at 1 kHz were measured using a HP 4284A precision LCR meter at different temperatures. Measurements of the microwave properties (up to 26 GHz) were performed at Chalmers University of Technology, which was one of the MELODY project partners, using an LTCC structure and a network analyzer (Paper V, Section 4.3.1).

## 4 Results and discussions

### 4.1 LTCC powders based on BST

Reduction of the sintering temperature of BST from 1350 °C to around 900 °C would allow integration of BST components with commercial dielectric LTCC layers and enable the use of silver electrode. This section is concerned with the low-temperature sintering of BST. First, the powders obtained via the sol-gel route are discussed, and second, those derived via the mixed-oxide route to which sintering aids were added are presented.

#### 4.1.1 *BST and BSTB powders prepared by the sol-gel method*

The sol-gel process was used to prepare BST powders, which are characterized by ultrafine homogeneous powders with large specific surface areas and high reactivity. Such highly reactive powders usually offer lower sintering temperatures compared to conventional ‘mixed-oxide’ materials (Wang 1976, Lee & Pope 1994). The main purpose was to study the sintering temperature of pure BST and B<sub>2</sub>O<sub>3</sub>-added BST powders prepared by the sol-gel method. B<sub>2</sub>O<sub>3</sub> is known to be an effective sintering aid; it reacts with the functional hydroxyl group in polyvinyl butyral and leads to the development of a 3-dimensional gel (Cho *et al.* 2003, Su & Button 2001). This makes B<sub>2</sub>O<sub>3</sub>-added BST powders difficult to use in the tape casting process.

Three powders were prepared via the sol-gel route, and all had small particle size and larger specific surface areas. The SSA values of the BST-sg, BSTB1-sg and BSTB2-sg (Table 2) powders were 18.7, 6.8 and 6.7 m<sup>2</sup>g<sup>-1</sup> respectively, whereas the powder made by the mixed-oxide route (BST-o) had SSA of 3.0 m<sup>2</sup>g<sup>-1</sup>.

The DTA/TGA and XRD measurements showed the growth of the perovskite Ba<sub>0.7</sub>Sr<sub>0.3</sub>TiO<sub>3</sub> phase at 700 °C, and a small number of secondary phases of (BaO)(B<sub>2</sub>O<sub>3</sub>) and/or BaTi(BO<sub>3</sub>)<sub>2</sub> were formed at 967 °C but disappeared above 1200 °C. Boron was

present in the glassy phase, not found in XRD, at low temperatures and then formed a secondary phase or evaporated during the sintering (Paper I).

Fig. 8 shows that the densification behaviours of the BST-o and BST-sg powders were almost identical. The sol-gel powder having the larger SSA did not shrink as much as expected. This is due to the resultant ineffective filling of space in the powder compact and the consequent high porosity of sintered ceramics and also to the nonstoichiometry of the sol-gel powder.

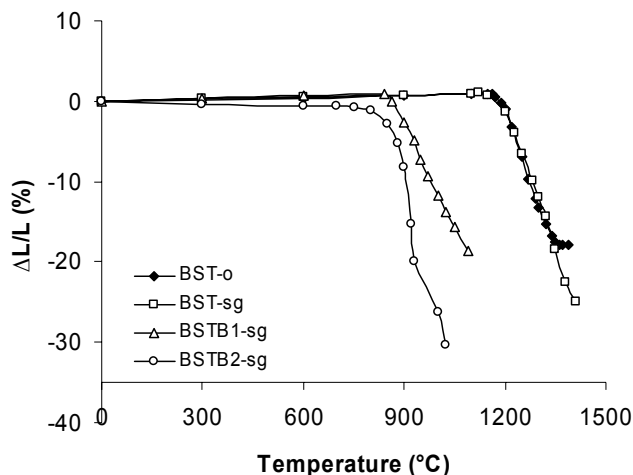


**Fig. 8. Sintering behaviours of BST and BSTB compacts (Paper I).**

Effective sintering of BSTB occurred at 1000 °C and 900 °C for BSTB1-sg and BSTB2-sg, respectively. Although the amount of  $B_2O_3$  was much higher in BSTB2-sg than in BSTB1-sg, sintering temperature was not lowered as much as expected. The  $B_2O_3$  added to BSTB2-sg might partly evaporate from the bulk or remain in a glassy form.

Based on dielectric measurements (Fig. 9), the permittivity of BST-o showed typical temperature dependence, with the temperature of maximum permittivity around 305 K. The maximum permittivity of BSTB1-sg was half of the value of BST-o, and its dissipation factor was lower than BST-o (decreasing from 0.0102 to 0.0060 at room temperature). It is also significant that the  $T_c$  values for BST-o, BST-sg and BSTB1-sg were the same. For BSTB2-sg, however, no clear maximum permittivity as a function of temperature was evident due to the secondary phase that surrounds the grains and blocks the ferroelectric response, or probably because the grains are small and the structure porous (Paper I).

When BST powder is prepared by the sol-gel route, a larger amount of  $B_2O_3$  (6 wt%) can be added compared to conventionally prepared  $B_2O_3$ -added BST powders (Rhim *et al.* 2000), and further more the BSTB-sg powders can prevent the formation of 3-

dimensional gel caused by  $B_2O_3$ . The sintering temperature of BSTB2-sg was reduced from 1360 °C to 900 °C.

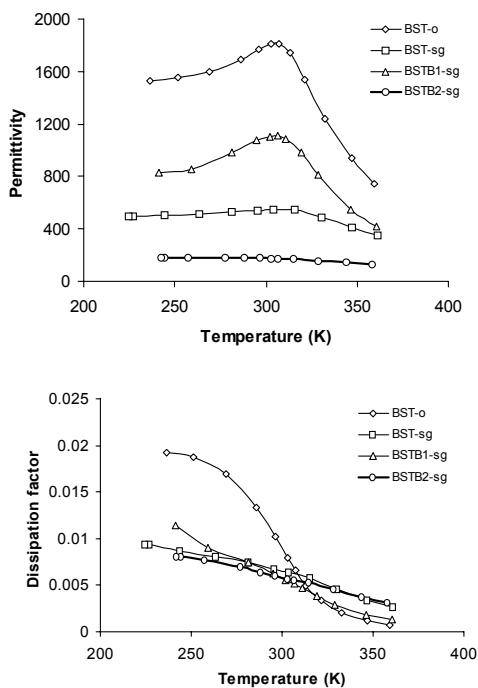


**Fig. 9. Dielectric properties of sintered BST and BSTB as a function of temperature (Paper I).**

The study described so far set out to assess the extent to which the sol-gel route was able to yield powders that are promising candidates for LTCC applications. Although the constraints on time did not permit the powders to be studied in detail, the indications were that a residual boron-based glass phase adversely affected the dissipation factor and permittivity. The dissipation factor was not low enough for microwave application. For this reason, the emphasis of the research was switched to powders derived by the mixed-oxide route and to a range of sintering aids.

#### **4.1.2 BST with sintering aids of $B_2O_3$ and $Li_2CO_3$**

Various additives were considered to lower the sintering temperature of  $Ba_{0.7}Sr_{0.3}TiO_3$ . These included  $B_2O_3$ ,  $Li_2CO_3$ ,  $Y_2O_3$ ,  $Bi_2O_3$  and  $CuO$  (Paper VI). Based on the shrinkage data following sintering at  $\sim 900$  °C and the amounts of additives used, attention was confined to the combination of  $B_2O_3$  and  $Li_2CO_3$ .

Pure  $Ba_{0.7}Sr_{0.3}TiO_3$  bulk ceramics were prepared as reference pieces. The pressed pellets sintered at 1360 °C had linear shrinkage of 12.7 %, mass loss of 2.0 wt% caused

by binder, water and release of CO<sub>2</sub> from Li<sub>2</sub>CO<sub>3</sub> and density of 5.4×10<sup>3</sup> Kg m<sup>-3</sup>. Table 3 shows the sintering behaviour of BST samples with different amounts of combined Li<sub>2</sub>CO<sub>3</sub> and B<sub>2</sub>O<sub>3</sub> additions after firing at different temperatures for 4 hours.

*Table 3. Shrinkages behaviour of BST with different amounts of B<sub>2</sub>O<sub>3</sub> and Li<sub>2</sub>CO<sub>3</sub> additions (Paper VI).*

Li <sub>2</sub> CO <sub>3</sub> +B <sub>2</sub> O <sub>3</sub> (wt%)	Ts (°C)	Shrinkage (%)	Mass Loss (wt%)	Fired Density (×10 <sup>3</sup> Kg m <sup>-3</sup> )	Code
0.0 + 0.0	1360	12.7	2.0	5.4	BST
3.5 + 4.0	850	11.9	4.5	4.2	L3
	900	14.8	4.5	4.6	
	950	15.7	4.5	4.7	
6.0 + 1.5	850	16.6	6.6	4.8	L4
	900	18.2	5.1	5.1	
7.5 + 0.0	850	11.3	3.5	4.5	L5
	900	11.9	4.5	4.5	
2.0 + 0.5	850	7.5	3.1	4.9	L6
	900	12.7	3.1	5.0	
2.0 + 1.0	850	11.6	3.0	4.5	L7
	900	14.3	3.5	4.8	
1.5 + 0.5	850	7.4	2.5	4.2	L8
	900	10.1	2.5	4.5	
2.5 + 0.5	800	12.0	4.0	4.5	L9
	850	15.6	3.5	5.1	
	900	16.5	4.0	5.2	
2.25 + 0.5	850	5.0	2.5	3.7	L10
2.25 + 0.75	850	9.7	3.5	4.2	L11
	900	13.9	3.5	4.8	
	910	15.6	3.5	5.1	
2.4 + 0.6	850	11.0	3.5	4.7	L12
	870	13.3	3.5	5.1	
	890	14.3	3.5	5.2	
2.32 + 0.68	850	10.9	3.5	4.8	L13
	870	13.6	4.0	5.2	
	890	14.5	4.0	5.4	
3.0 + 0.75	850	14.4	4.5	4.8	L14
	870	16.1	4.5	5.1	
	880	16.5	5.0	5.1	
2.55 + 0.7	850	9.3	3.5	4.2	L15
	870	12.0	3.5	4.6	
	890	13.5	3.5	4.8	
	900	14.2	3.5	4.9	

The mass loss values show that, at moderate addition levels, only a minor fraction of sintering aids evaporate during firing. It can be seen that Li<sub>2</sub>CO<sub>3</sub> alone (L5) did not allow

complete ceramic densification. Thus, several test compositions, such as L3, L4, L6, L7, L8 and L10, were prepared. The results show that there is a distinct optimal ratio of these sintering aids. The compositions L11–L14 were prepared to clarify this point, the  $\text{Li}_2\text{CO}_3 : \text{B}_2\text{O}_3$  ratios in wt% ranging from 3 : 1 to 4 : 1. All compositions produced samples with high final densities ( $>5 \times 10^3 \text{ Kg m}^{-3}$ ) after sintering near  $900^\circ\text{C}$  with a dwell time of 4 hours. In the  $\text{Li}_2\text{O}-\text{B}_2\text{O}_3$  phase diagram, a very low melting point phase can be seen at  $650^\circ\text{C}$  with a  $\text{Li}_2\text{O} : \text{B}_2\text{O}_3$  composition ratio in wt% of 0.9 : 1 (Levin *et al.* 1964), which gives theoretical support for the experimental results. However,  $\text{Li}_2\text{CO}_3$  was added in our experiments instead of  $\text{Li}_2\text{O}$ .

The best composition according to the sintering behaviour studies, denoted as L13, was achieved by 2.32 wt% addition of  $\text{Li}_2\text{CO}_3$  and 0.68 wt% addition of  $\text{B}_2\text{O}_3$  (ratio of 3.4 : 1). The measured density after sintering at  $890^\circ\text{C}$  was  $5.4 \times 10^3 \text{ Kg m}^{-3}$ , and the same value was obtained for pure BST bulks sintered at  $1360^\circ\text{C}$ . This is a much better result ( $T_s$  was  $260^\circ\text{C}$  lower) than that achieved for BST when only  $\text{B}_2\text{O}_3$  was added (Rhim *et al.* 2000, Paper I). After firing at  $890^\circ\text{C}$ , the microstructure of L13 was uniform without abnormal grain growth. The average grain size was in the range of  $1\text{--}8 \mu\text{m}$  (Paper VI). The phases detected by XRD were related to BST, with only one small unidentified peak. Thus, it can be said that the combined addition of  $\text{Li}_2\text{CO}_3$  and  $\text{B}_2\text{O}_3$  is more effective, especially when low sintering temperatures are required.

Furthermore, the presence of boron and lithium after sintering was studied by a PU7000 ICP (inductively coupled plasma) spectrometer (Philips, Netherlands). The results shown in  $\text{mg g}^{-1}$  of boron and lithium had been transformed into a weight percentage of  $\text{B}_2\text{O}_3$  and  $\text{Li}_2\text{CO}_3$ . The amounts of  $\text{B}_2\text{O}_3$  and  $\text{Li}_2\text{CO}_3$  in a sintered L13 sample were 0.45 wt% and 1.65 wt%, respectively. Thus, although some evaporation took place, boron and lithium still remained in the sintered samples. With regard to these results and the sintering behaviour measurements, it can be assumed that  $\text{B}_2\text{O}_3$  and  $\text{Li}_2\text{CO}_3$  first form a liquid phase enhancing low-temperature shrinkage through liquid phase sintering and later, at higher temperatures, evaporate to some extent, and  $\text{Li}_2\text{CO}_3$  decomposes or reacts with  $\text{Ba}_{0.7}\text{Sr}_{0.3}\text{TiO}_3$  into  $\text{Li}_2\text{O}$  or  $\text{Li}_2\text{TiO}_3$ , leaving behind the microstructure of an almost pure BST phase. The residual boron and lithium might reside at grain boundaries or in a glass form, which can not be detected by XRD.

The permittivity and dissipation factors at 1 kHz as functions of temperature for pure BST and for two low sintering temperature compositions (L13 and L14) fired at  $890^\circ\text{C}$  and  $870^\circ\text{C}$ , respectively, are shown in Fig. 10.

The total added amount of 3 wt% of  $\text{Li}_2\text{CO}_3$  and  $\text{B}_2\text{O}_3$  (L13) decreased permittivity to 4290 compared to the pure BST value of 4970. This level of sintering aid addition did not change the phase transformation behaviour, no transition broadening was observed, and  $T_c$  was the same as for pure BST (310 K). The dissipation factors for BST and L13 were the same (0.005) at  $T_c$ , but at low temperatures the addition of sintering aids was beneficial. In contrast, in the case of a higher dopant level (L14; 3.75 wt%), the Curie peak was almost totally suppressed, and the dissipation factor markedly increased.

$\text{Ba}_{0.7}\text{Sr}_{0.3}\text{TiO}_3$  with 3 wt%  $\text{Li}_2\text{CO}_3$  and  $\text{B}_2\text{O}_3$  showed good dielectric properties but too high permittivity for application as a microwave tunable device (desired  $\epsilon_r$ : 100–1000). Furthermore, the paraelectric state of BST is needed. Therefore, the BST composition was altered as described in the following section.

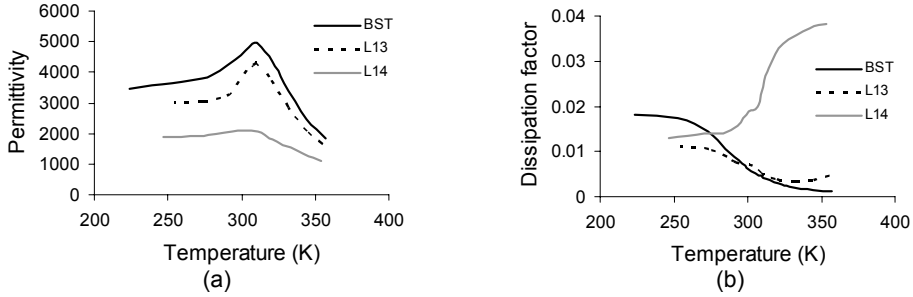


**Fig. 10. (a) Permittivity and (b) dissipation factors as functions of temperature for pure BST and for two low sintering temperature compositions (L13 and L14) (Paper VI).**

### 4.1.3 BSTM with sintering aids of $B_2O_3$ and $Li_2CO_3$

The study so far described was concerned with fluxed BST-based composition. Initially, BST powders prepared by the sol-gel route were examined, but because the dissipation factor was not low enough for microwave application, attention was turned to powders prepared by the mixed-oxide route. Various fluxing agents were considered and, following exploratory experiments, attention was focussed on combinations of  $Li_2CO_3$  and  $B_2O_3$ . Although good-quality ceramics were produced at the appropriate sintering temperature for LTCC applications, the permittivity values were considered too high. Attention was then turned to fluxing a recently developed base MgO-BST composition ( $0.4Ba_{0.55}Sr_{0.45}TiO_3-0.6MgO$ , designated as ‘BSTM’), which shows promising dielectric properties for the envisaged applications. This base material has a room temperature permittivity of 511 at 1.3 GHz. The reduction in the permittivity of MgO-BST is partly due to the replacement of some (~2 at%) of the  $Ti^{4+}$  by the slightly larger and lower charged  $Mg^{2+}$  ion, which could be expected to reduce the overall crystal polarizability, and partly to the general permittivity dilution according to Lichtenecker’s rule and, further, to the location of the low permittivity phase at the grain boundaries. The experimental work is discussed below.

Based on the experience gained from the work described above, the basic BSTM powder, supplied by the project partner Filtronic Comtek Ltd. (UK) and prepared by the mixed-oxide route, was fluxed with combinations of  $Li_2CO_3$  and  $B_2O_3$  (Paper IV). The amounts of sintering aids,  $Li_2CO_3$  and  $B_2O_3$ , were varied, and the ratio of  $Li_2CO_3$  and  $B_2O_3$  was held constant at 5 : 1 (Table 4). Additive optimization was determined from data on the fired density, sintering behaviour, microstructure and dielectric properties of the bulk ceramics at 1 kHz.

Based on shrinkage behaviour, the sintering temperatures for the different compositions chosen for further study were determined by choosing temperatures that corresponded to shrinkage of ~17 % in the XY direction. The densities and shrinkages in the XY and Z directions for each composition were measured after sintering (Table 4). These results also showed that a single addition of  $B_2O_3$  or  $Li_2CO_3$  alone did not

sufficiently decrease the sintering temperature. In one case (BSTM-B), acceptable shrinkage occurred only after sintering at 1140 °C, and in another (BSTM-L), full density was not achieved till 1200 °C, as expected based on the shrinkage data.

*Table 4. Sintering behaviour for different boron and lithium concentrations (Paper IV).*

	B <sub>2</sub> O <sub>3</sub> (wt%)	Li <sub>2</sub> CO <sub>3</sub> (wt%)	Sintering Temp. (°C)	Density (10 <sup>3</sup> Kg m <sup>-3</sup> )	ρ/ρ <sub>o</sub> * (%)	Shrinkage	
						XY (%)	Z (%)
BSTM	0	0	1400	4.78	97.2	16.5	16.0
BSTM-B	0.50	0	1140	4.43	90.4	15.9	15.9
BSTM-L	0	2.5	1200	3.96	83.2	12.3	11.8
BSTM-BL1	0.25	1.25	1080	4.35	90.1	17.2	16.7
BSTM-BL2	0.5	2.5	1050	4.35	91.8	17.4	16.6
BSTM-BL3	0.75	3.75	950	4.23	90.8	17.5	16.2
BSTM-BL4	1.00	5.00	920	3.70	81.0	16.7	16.9

\* Percentage of measured density relative to theoretical density

The addition of both Li<sub>2</sub>CO<sub>3</sub> and B<sub>2</sub>O<sub>3</sub> in moderate amounts resulted in good fired densities. When a total amount of 4.5 wt% dopant was added, a final density of 90.8 % of the theoretical density was achieved at the low sintering temperature of 400 °C. The XRD data (Fig. 11) show that the major phases developed in all samples were BaSrTiO<sub>3</sub> and MgO with no significant amounts of other crystalline phases. With larger amounts of additives (>6 wt%), however, a small unidentified peak (marked "?") was detected at approximately 2θ = 30°.

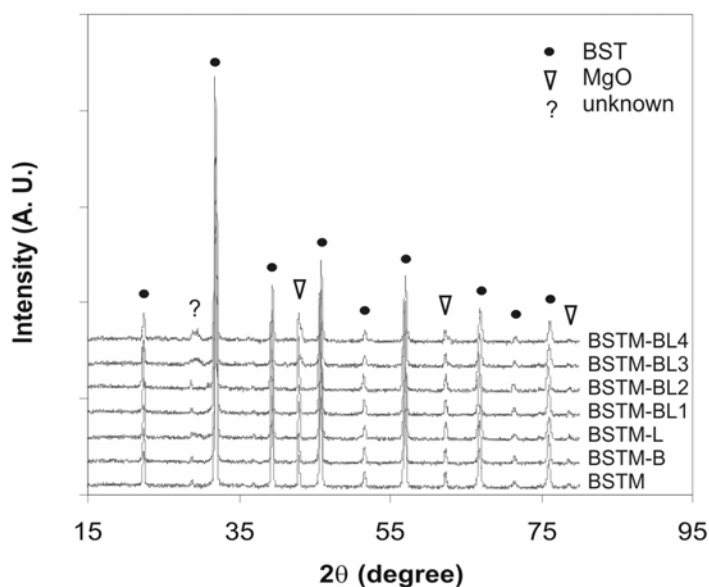


**Fig. 11. XRD patterns for different B<sub>2</sub>O<sub>3</sub> and Li<sub>2</sub>CO<sub>3</sub> concentrations (Paper IV).**

The microstructures revealed by SEM (Fig. 12 and Paper IV) were all uniform without large pores, except when only  $\text{Li}_2\text{CO}_3$  was added. Each micrograph showed grey and dark areas, shown by EDS to be pure BST and MgO phases, respectively. Only after the addition of a large amount ( $>4.5$  wt%) of sintering aids did new light areas appear (Paper IV). The EDS analyses showed this phase to be composed of BST enriched with barium. The observations confirm that  $\text{B}_2\text{O}_3$  and  $\text{Li}_2\text{CO}_3$  act as effective sintering aids leading to pore-free microstructures with no evidence of minor phases.

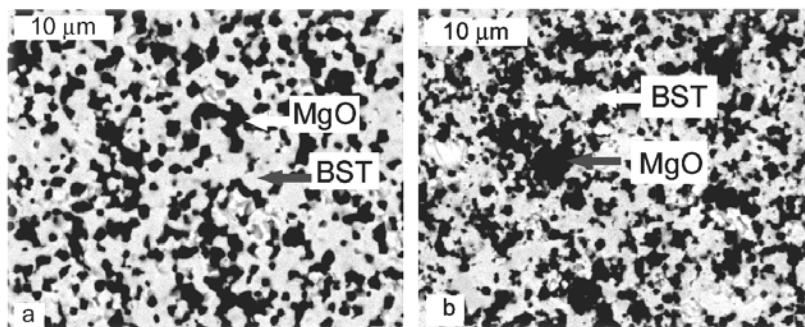


**Fig. 12. SEM/BE images of (a) BSTM sintered at 1400 °C, (b) BSTM-BL3 at 950 °C with dwell times of 2 hours (Paper IV).**

The permittivity and dissipation factor values for all compositions, measured as a function of temperature at 1 kHz, are shown in Fig. 13. The permittivity and dissipation factors for BSTM at  $T_c$  209 K were 1914 and 0.0021, respectively; at 293 K (room temperature) the corresponding values were 569 and 0.0015, which are consistent with the values reported by others (Sengupta *et al.* 1995, Sengupta & Sengupta 1999, Ngo *et al.* 2001). For  $\text{Ba}_{0.60}\text{Sr}_{0.40}\text{TiO}_3$  with 20 wt% MgO, the values given by Sengupta *et al.* are approximately 886 and 0.0010 for permittivity and dissipation factor, respectively, and 16 for tunability (applied electric field  $2.27 \text{ V } \mu\text{m}^{-1}$ ) measured at 1 kHz and room temperature.

The best results for dielectric property were obtained following a total addition of 4.5 wt%  $\text{B}_2\text{O}_3$  and  $\text{Li}_2\text{CO}_3$  (BSTM-BL3), which led to sintering temperature values of 950 °C, permittivity of 221 and a very low dissipation factor of 0.0012 at 293 K. At the Curie temperature of BSTM-BL3 124 K, permittivity was 615 and dissipation factor 0.0047. When lower dopant additions were made (BSTM-BL1 and BSTM-BL2), the sintering temperature was too high ( $>1000$  °C) for the LTCC process, and larger amounts of sintering aids (BSTM-BL4) destroyed the dielectric properties. The optimized amount of sintering aids for BSTM (4.5 wt%) is larger than that for pure BST (3 wt%) (Section 4.1.2) due to the MgO addition. The BSTM-BL3 composition was used for making tape and microwave measurement structure.

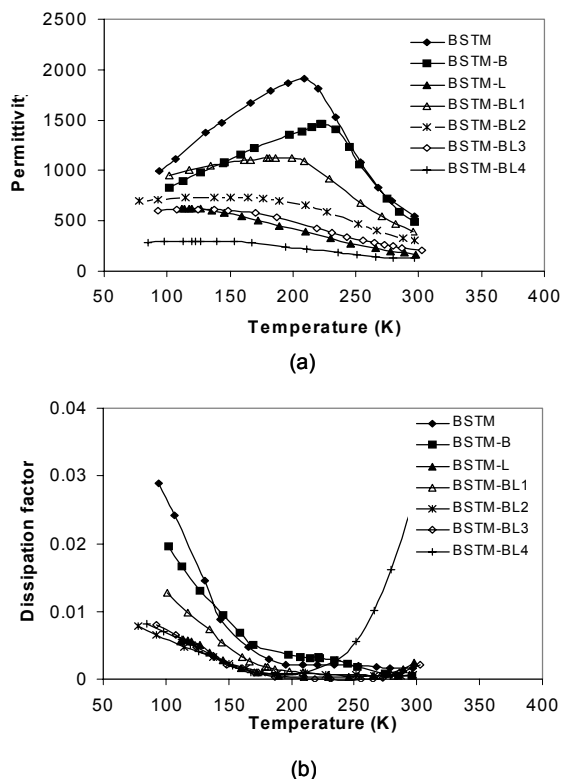


Fig. 13. (a) Permittivity and (b) dissipation factors at 1 kHz for different compositions as functions of temperature (Paper IV).

## 4.2 Fabrication of tapes and laminates

Powder characteristics, organic additives, viscosity of slurry and casting parameters, all in turn, influence the characteristics of tape (Mistler & Twiname 2000). In the present study, the single slurry system, as described in Section 3.2, was used. Taking into account the general requirements of the tape manufacturing process along with the demands for density, strength and flexibility, the appropriate amounts of additives and solvents (Table 5) for each powder were adjusted and optimized experimentally.

BST powders prepared by the sol-gel process were also used to make tape and compared with powder by the conventional mixed-oxide method (Paper II). TEM images of the sol-gel powder indicated that the particle size of BST-sg was 0.05–0.1  $\mu\text{m}$ , which is finer than BST-o (approximately 0.6–1.5  $\mu\text{m}$ ). The mean tensile strength values of BST-o and BST-sg green tapes were 2.96 MPa and 4.29 MPa, respectively. The tape made from sol-gel powder was stronger, which can be explained partly by the larger surface area of the powder and partly by the larger amount of binder needed. The surface

roughness of BST-sg green tape was 0.15  $\mu\text{m}$  and that of BST-o 0.20  $\mu\text{m}$ , both of which are smaller than those reported for commercial ceramic tapes, 0.4  $\mu\text{m}$  (Kulke *et al.* 2001).

Table 5. Slurry compositions for different ceramic powders (wt%) (Paper II, III).

	Powder	Ethanol	Xylene	Fish oil	B98	S160	Ucon
BST-o	60.0	16.5	16.5	1.2	3.8	1.0	1.0
BST-sg	50.0	14.0	28.0	1.5	4.5	1.0	1.0
BST-BL	50.0	19.0	19.0	1.3	3.7	0.9	0.9
BSTM-BL	50.0	17.0	17.0	1.2	4.0	1.0	1.0
PZT	62.6	11.7	17.6	0.9	4.8	1.2	1.2
NZF	60.0	16.1	16.1	1.2	4.4	2.2	0
ZSB	55.8	18.5	18.5	1.1	4.1	1.0	1.0

Several layers of green tapes were laminated at 70 °C and 15 MPa for 20 minutes and then sintered at different temperatures. After sintering at 1250 °C, both BST-o and BST-sg tapes had porous microstructures with low measured densities of  $3.9 \times 10^3$  and  $3.8 \times 10^3 \text{ Kg m}^{-3}$ , respectively. However, the tapes formed with BST-sg powder showed greater shrinkage in all directions than those with BST-o powder. The experiments showed that BST-o powder required a minimum temperature of 1300 °C to achieve good sintering. In contrast, BST-sg laminates could not be successfully sintered at 1300 °C because of excessive grain growth and the development of large pores and blistering. The evidence indicates that, in the case of BST-sg powder, a sintering temperature of slightly above 1250 °C would be sufficient, and that close attention should be given to the burn-out of the organic compounds and the overall firing schedule.

It was found that the amount of sintering aids had to be increased because of the organic additives in the slurry composition. The binder and plasticizer retained in the green tape influenced the amount of sintering aids. After sintering at 900 °C, the BST-BL ( $\text{Ba}_{0.55}\text{Sr}_{0.45}\text{TiO}_3$  added 4.5 wt%  $\text{B}_2\text{O}_3$  and  $\text{Li}_2\text{CO}_3$ ) multilayer stack achieved a density of  $4.9 \times 10^3 \text{ Kg m}^{-3}$  with shrinkages of 19.2 % in the XY and 18.3 % in the Z direction. When the sintering temperature was raised to 950 °C, density increased to  $5.1 \times 10^3 \text{ Kg m}^{-3}$ . In the case of  $\text{Ba}_{0.55}\text{Sr}_{0.45}\text{TiO}_3$ , without fluxing additives and sintered at 1400 °C, a density of  $5.6 \times 10^3 \text{ Kg m}^{-3}$  was achieved. Additionally, SEM images of the sintered laminate also confirmed the presence of a dense, uniform microstructure with low porosity. The BSTM-BL ( $0.4\text{Ba}_{0.55}\text{Sr}_{0.45}\text{TiO}_3-0.6\text{MgO}$  with 4.5 wt%  $\text{B}_2\text{O}_3$  and  $\text{Li}_2\text{CO}_3$ ) based multilayer structure was made by laminating 10–15 layers of green tape at 70 °C 20 MPa for 20 minutes. After sintering at 950 °C, the density of the multilayer structure was  $4.0 \times 10^3 \text{ Kg m}^{-3}$ , which is 95 % of the density of BSTM sintered at 1400 °C.

Because of the experience gained and its relevance to the exploitation of other important electroceramics, some subsidiary experiments were carried out on a piezoceramic, a ferrite and a dielectric used for future LTCC modules (Fig. 2). The composition of barium strontium titanate (BST-o) used in this work was  $\text{Ba}_{0.7}\text{Sr}_{0.3}\text{TiO}_3$ . Lead zirconate titanate (PZT) is a piezoelectric ceramic used in actuators, sensors and transformers (De Vries *et al.* 1996). The ferrimagnetic ceramic was  $\text{Ni}_{0.55}\text{Zn}_{0.5}\text{Fe}_{1.85}\text{O}_x$  (NZF), which is commonly used for magnetic cores. The LTCC dielectric  $\text{MgTiO}_3\text{-CaTiO}_3\text{-ZnO-SiO}_2\text{-B}_2\text{O}_3$  (ZSB) is exploited in capacitors, resonators and filters (Jantunen

*et al.* 2001). The measured SSA of the starting powders, BST-o, PZT, NZF and ZSB, were 3.0, 1.0, 4.9 and 2.6 m<sup>2</sup>g<sup>-1</sup> respectively, and the corresponding mean particle sizes were 1.2, 3.6, 0.5 and 1.8 μm, respectively. These characteristics are suitable for tape-casting (Mistler & Twiname 2000). The slurry compositions, given in Table 5, were optimized for each system (Paper III).

The tapes were cast, and 10-20 layers of green tape were laminated at 70 °C, 15–20 MPa, with dwelling times of 15–20 minutes. The laminates were fired to schedules ensuring safe removal of organics and to peak temperatures necessary to effect complete sintering (BST-o: 1300 °C, PZT: 1050 °C, NZF: 1300 °C, ZSB: 900 °C). The apparent porosity values of the sintered BST-o, PZT, NZF and ZSB were 2.3, 2.5, 5.7 and 0.6 vol%, respectively. The shrinkage values that lay in the range of 14.8–18.7 % (XY direction) and in the range of 10.5–19.0 % (Z direction) did not correlate with the amounts of solvents or slurry additives.

The surfaces of sintered BST-o and PZT were smooth with RA values of 0.2 μm. However, in the case of NZF (RA=0.5 μm) and ZSB (RA=0.6 μm), there was some structural coarsening. ZSB had a polyphased microstructure (Jantunen *et al.* 2001).

## 4.3 Microwave measurements

### 4.3.1 Microwave characterization

Measurement of the dielectric properties of high-permittivity ceramics, especially under external DC bias at microwave frequencies, is a challenging problem. Most of the reported methods are based on hollow waveguides (coaxial lines) (Grigas 1996) and cavity resonators. They are useful in narrow frequency bands and generally cannot be used for measurements under applied DC bias, since such measurements require metal electrodes. A special method and test structures (Fig. 14) were developed to enable measurements in a wide frequency range using coplanar microprobes provided by Chalmers University of Technology, Sweden. Two test structures, 2.4 mm and 3.2 mm in length (L), were used for the frequency range 2–26 GHz. In the test structure, the BST LTCC layer (50 μm in thickness) was laminated (70 °C and 15 MPa for 20 minutes) onto a Pt electrode carried on alumina (99.6 %, 1 mm thick) and sintered at 950 °C subsequently. On the top of the surface, Ag coupled microstrip lines, 200 μm wide and 200 μm apart from each other, were screen-printed and post-fired (Paper V).

Because the BSTM-BL3 tape requires a sintering temperature of 950 °C, platinum was chosen as the bottom electrode. For more optimized composition (BST-BL), having a sintering temperature of 875 °C, silver was used as the bottom electrode. Fig. 15 shows the microstructure of the fired LTCC layer (BSTM-BL3) on the alumina substrate.

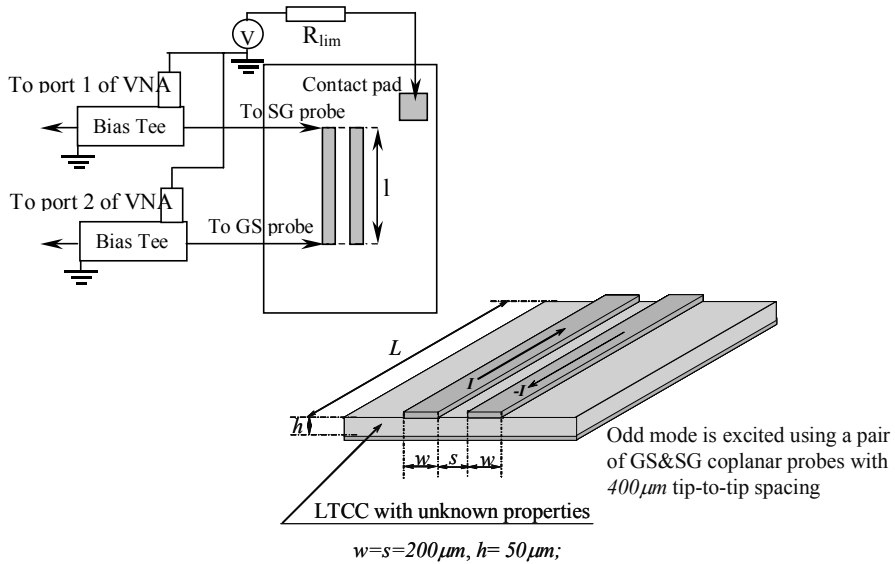


**Fig. 14. Set-up for measurement and layout of the test structure and (Paper V).**

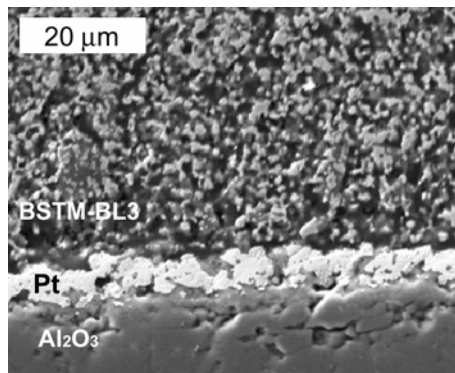


**Fig. 15. SEM/SE cross-section image of the multilayer structure for high-frequency measurement (Paper IV).**

Typical measured data for BSTM-BL3 layer are presented in Fig. 16a and 16b for 100 V and 200 V applied voltages, corresponding to  $2\text{ V } \mu\text{m}^{-1}$  and  $4\text{ V } \mu\text{m}^{-1}$  DC fields. Tunability was greater than 15 % over the entire frequency band, which is sufficient for the development of practically important tunable/adjustable components (Paper V). Relative permittivity at 26 GHz was 130 at room temperature without applied voltage.

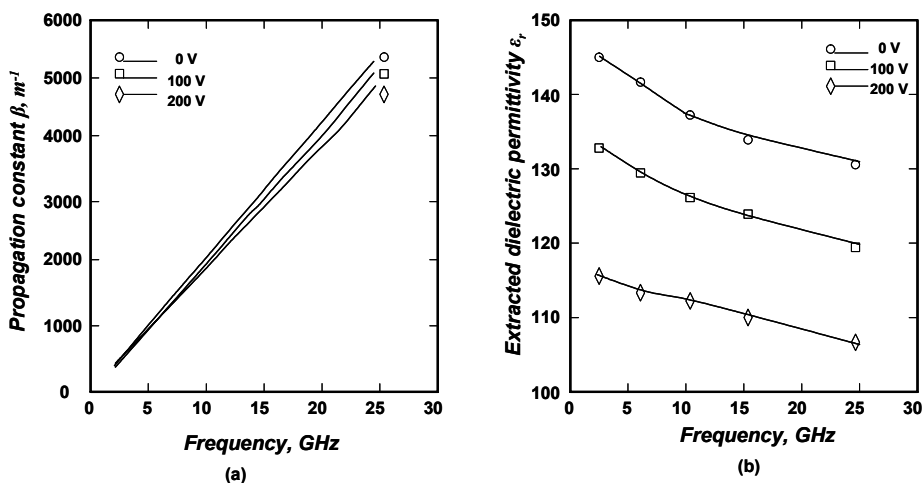


Fig. 16. (a) Measured propagation constant, (b) extracted dielectric permittivity (Paper IV).

### 4.3.2 Phase-shifter

The phase-shifter, designed at Chalmers University of Technology, is an example of microwave devices based on the properties of BSTM-BL3. The component was prepared on a 1 mm thick alumina substrate (99.6%), on which a BST LTCC layer 50  $\mu m$  in thickness was laminated and sintered at 950  $^{\circ}C$ . The conductive patterns were silver-printed by the direct gravure printing technique, which allows 20  $\mu m$  line widths and gaps with sintered thickness  $>5 \mu m$  (Kittilä *et al.* 2003).

The phase-shifter is a conductive line periodically loaded by lumped capacitors (Fig. 17) with input and output quarter wavelength matching networks. The measured S-parameters of a phase-shifter under DC bias of 50, 75, 100 and 125 V are shown in Fig. 18a. Fig. 18b shows the differential phase shift under different bias voltages. The component at 26 GHz demonstrated a phase shift from 10 to 35 $^{\circ}$  when the voltage over the gap was increased from 50 V to 125 V.

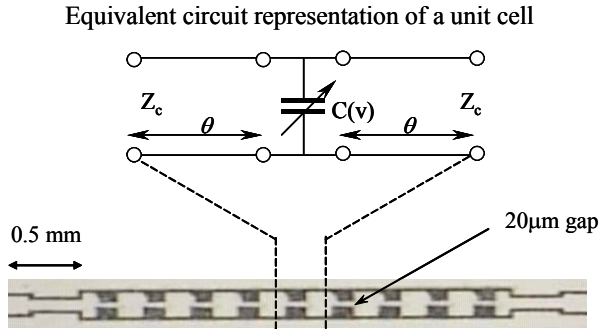


Fig. 17. Photograph and equivalent circuit of the phase-shifter.

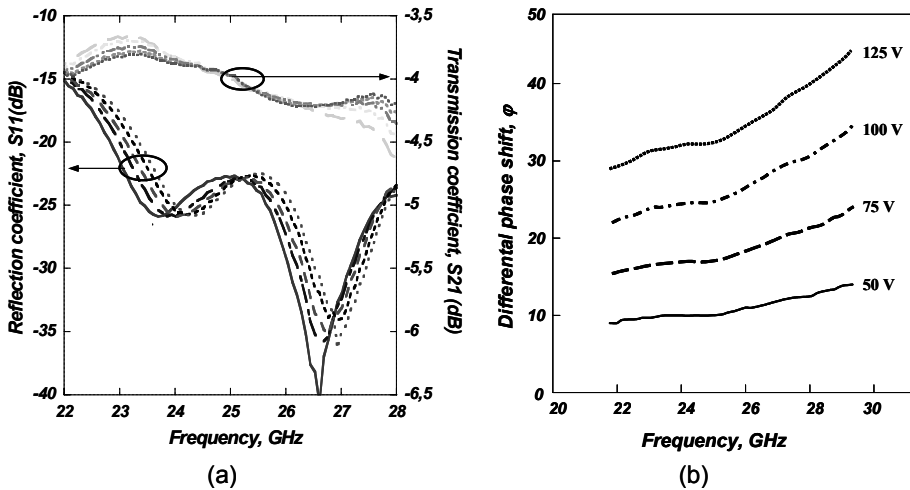


Fig. 18. (a) S-parameters of the phase-shifter and (b) differential phase shift under 50, 75, 100 and 125 V.

In order to gain experience with the newly developed compositions in the multilayer circuit context, some exploratory experiments were conducted. One such example is illustrated in Fig. 19.

Fig. 19a shows the bottom pattern of a device screen-printed on an alumina substrate (Dupont 7760 silver paste). After laminating the LTCC (BST-BL) green tape onto the substrate, vias were laser-drilled and then filled with Dupont 6141 silver paste. After that, the direct gravure printing approach was used to print Dupont 6145 conductor paste. Co-firing was carried out at 875 °C for 4 hours. The surface conductor patterns are shown in Fig. 19b and 19c. Fig. 19d shows a cross-section of the fired structure, in which the BST layer was 50  $\mu$ m thick. The thickness of the silver lines printed by the screen printing or

direct gravure printing method was around  $8\ \mu\text{m}$ . Analyses of the microwave measurements are in progress.

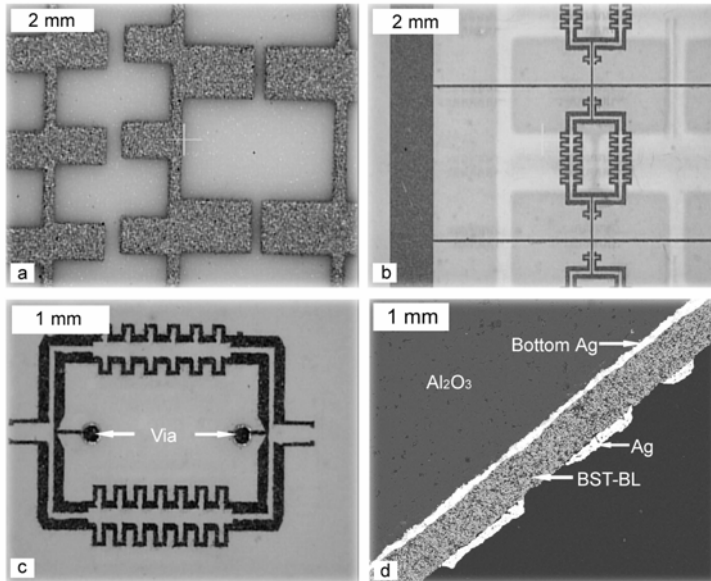


Fig. 19. Images of (a) bottom silver, (b-c) upper silver patterns, and (d) cross-section.

#### 4.4 Co-firing of BST-BL tape with other tapes

BST-BL tapes were laminated with several commercial dielectric LTCC tapes and co-fired (Hu *et al.* 2003). The properties of the commercial dielectric LTCC tapes (Table 6) were obtained from the technical data sheets of the products from DuPont Microcircuit Materials, Ferro Corporation: Electric Materials Division, and W.C. Heraeus GmbH & Co. KG: Circuit Material Division. The shrinkage, density, RA and coefficient of thermal expansion (CTE) of BST-BL laminate were measured after sintering at  $875\ ^\circ\text{C}$  for 4 hours. The CTE values indicate that the BST-BL tapes show greater thermal expansion than the commercial dielectric LTCC tapes. The shrinkage of the BST-BL tape was greater than that of DP951, DP943 and CT2000, but smaller than that of FerroA6-S. The differences in CTE and shrinkage between different tapes cause difficulties in the co-firing of commercial LTCC and the BST-BL tapes.

Table 6. Properties of tapes (source: data sheets of the products).

	Surface RA fired ( $\mu\text{m}$ )	Tensile strength (MPa)	CTE (ppm/ $^{\circ}\text{C}$ )	Green Density ( $10^3\text{Kg m}^{-3}$ )	Flexural Strength (MPa)	Sintered Density ( $10^3\text{Kg m}^{-3}$ )	Shrinkage XY, Z (%)
BST-BL	0.4	1.7	11.7	3.2	-	4.9	18.7, 17.1
DP951	<0.2	1.7	5.8	-	320	3.1	12.7, 15.0
DP943	0.7	2.0	4.5	2.4	230	3.2	9.5, 10.3
CT2000	<0.2	1.7	5.6	2.3	310	3.1	10.6, 16.0
Heraclon	<0.7	1.7	6.1	2.3	250	2.9	0.2, 22.6
FerroA6-S	-	-	>8	-	>160	2.4	15.3, 24.0

Sandwich structures of the various LTCC/BST/LTCC combinations were laminated at 70  $^{\circ}\text{C}$  and 20 MPa for 25 minutes and then co-fired at 875  $^{\circ}\text{C}$  for 1–4 hours. The DuPont tape DP951 was first co-fired with  $\text{Ba}_{0.7}\text{Sr}_{0.3}\text{TiO}_3$  tape (L13) (Paper VI). Co-firing produced dense microstructures of the dielectric material, but the BST-BL layer showed excess porosity compared to the bulk samples. At the interface between BST-BL and DP951, a mixed element zone with a thickness in the range of 8.2–8.8  $\mu\text{m}$  was observed. One explanation is the difference between the sintering properties of the tapes. During firing, when the dielectric tape has reached its full density and no more shrinkage in the XY direction takes place, this may constrain the shrinkage of the BST-BL tape. Co-firing of Heraeus CT2000 layers with BST-BL showed the same situation as DP951. The CT2000 tapes reach their full density earlier and restrict the release of the pores from the BST-BL layer. Co-firing of BST-BL with FerroA6 showed evidence of excessive interdiffusion. The sintered ceramic consisted of large pores in a dense matrix; this might be due to the movement and evaporation of  $\text{B}_2\text{O}_3$ .

Co-firing of BST-BL with Heraclon and DP943 tape yielded promising results. In Fig. 20a, it can be seen that the BST-BL layer has a dense and good microstructure even when the Heraclon layers are porous. The regular pores in the XY direction can be seen in the Heraclon tape, and evaporation in some compositions was estimated. Dupont 943 tape laminated with BST-BL (Fig. 20b) showed that the BST-BL layer was dense with no interdiffusion between the layers, and the Dupont dielectric was slightly porous.

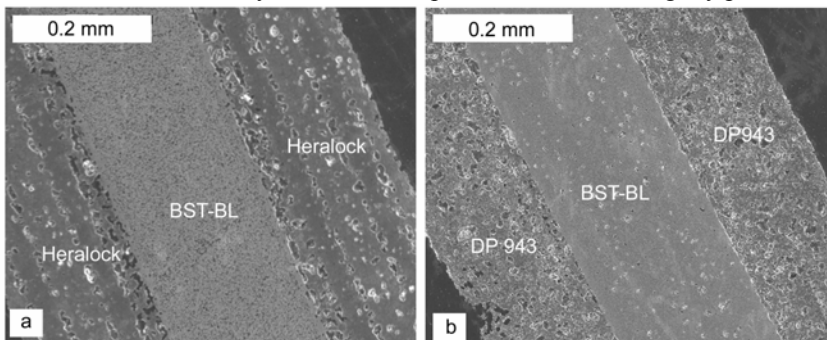


Fig. 20. Cross-section images of co-fired BST-BL in between commercial dielectric LTCC tapes (a) Heraclon, (b) Dupont 943 (Hu *et al.* 2003).

Experiments were carried out to test the compatibilities of the BST-based layers with other electroceramics important in the LTCC context and listed in Table 6 of Paper III. The results showed that the interfaces of the different layers were clear without any delamination. As there were some differences in shrinkage, density and thermal expansion between BST and NZF, the co-fired ceramic multilayer showed some cracking and curling.

Further studies of the co-firing of different tapes are necessary in order to realize the type of the complex novel multilayer shown schematically in Fig. 2. In particular differences in the tape shrinkage and thermal expansivity of the different ceramics will need to be studied in detail, so as to minimize the risk of cracking and/or warping.

## 5 Conclusion

The thesis had as an objective the development of a BST-based LTCC suited to exploitation in microwave tunable components. Guided by the literature, the work focussed upon the perovskite type ferroelectric, barium titanate, for which the ferroelectric to paraelectric transition (the Curie Point  $T_c$ ) occurs at approximately 130 °C. By adding strontium titanate, which also has the perovskite structure and a transition temperature estimated to be near 0 K, the transition temperature of the solid solution (BST) can be adjusted.

For the applications envisaged, relative permittivity is required to be low (100–1000) and adjustable by a suitable applied electric field, the dielectric losses at room temperature must be small (dissipation factor  $\sim 0.001$ ) and, most importantly, the sintering temperature must be suited to the LTCC multilayer technology, i.e., in the region of 900 °C. The composition suited to the objectives is  $\text{Ba}_{0.7}\text{Sr}_{0.3}\text{TiO}_3$  and this, fluxed to lower the sintering temperature from approximately 1360 to  $\sim 900$  °C, was the basis for the study.

Initially, it was considered that sol-gel derived powders (BST-sg) would offer advantages over powders produced by the more common mixed-oxide method. These advantages of the sol-gel powders were believed to be high purity, molecular-scale homogeneity, enhanced reactivity, fine particle size and narrow size distribution. In order to lower the sintering temperature,  $\text{B}_2\text{O}_3$  was added to the BST-sg powder. The dissipation factor for the sol-gel powder was 0.006, which was smaller than that for the BST-o powder made by the mixed-oxide method but not low enough for the desired microwave devices. Therefore, the BSTB powders were not used for further component preparation.

In the light of the difficulties experienced with the sol-gel powders, attention was turned to the BST powders prepared by the mixed-oxide method and additions of  $\text{Li}_2\text{CO}_3$  and  $\text{B}_2\text{O}_3$  to suitably reduce the sintering temperature.

The sintered density of  $\text{Ba}_{0.7}\text{Sr}_{0.3}\text{TiO}_3$  with a 2.32 wt% addition of  $\text{Li}_2\text{CO}_3$  and 0.68 wt% addition of  $\text{B}_2\text{O}_3$  (L13, Table 3) after sintering at 890 °C was identical to that of pure  $\text{Ba}_{0.7}\text{Sr}_{0.3}\text{TiO}_3$  sintered at 1360 °C ( $5.4 \times 10^3 \text{ Kg m}^{-3}$ ). The microstructure was uniformly dense with no detectable secondary crystal phases. Permittivity was reduced,

and the dissipation factor at room temperature was approximately the same as that of  $\text{Ba}_{0.7}\text{Sr}_{0.3}\text{TiO}_3$  and even lower at lower temperatures (250 to 300 K).

The permittivity of L13 was still too high for microwave applications, and MgO was used to lower this property to the desired range. The ceramic, made by the mixed-oxide route, had the composition  $0.4\text{Ba}_{0.55}\text{Sr}_{0.45}\text{TiO}_3\text{-}0.6\text{MgO}$ . This base material has a room temperature permittivity of approximately 500 at 1.3 GHz, and it was expected that this value would be further reduced by the addition of the sintering aids necessary for LTCC application. Addition of 0.75 wt% of  $\text{B}_2\text{O}_3$  and 3.75 wt% of  $\text{Li}_2\text{CO}_3$  to  $0.4\text{Ba}_{0.55}\text{Sr}_{0.45}\text{TiO}_3\text{-}0.6\text{MgO}$  produced dense uniform bulk ceramics at sintering temperatures as low as 950 °C. At 1 kHz, the permittivity of the bulk ceramic was 221 and the dissipation factor was 0.0012 at 293 K.

In parallel with the work to optimize the BST-based LTCC, experiments were undertaken to develop slurries for suitable tape-casting. Tapes were successfully laminated, and the optimum burn-out and sintering schedules were determined.

Having identified a suitable BST-based material and optimized its sintering characteristics for LTCC technology, attention turned to exploratory experiments testing the material in actual devices.

A novel measurement structure was developed to measure the permittivity and electric field-induced ‘tunability’ of the BST-based LTCC over a frequency range of 2–26 GHz under applied electric fields of 0, 2 and 4  $\text{V } \mu\text{m}^{-1}$ . The relative permittivity values lay in the approximate range of 100–150, the precise values being dependent upon the applied field and frequency.

A microwave phase-shifter was fabricated based on the ‘in-house’ developed LTCC and gravure printing. A phase shift of 10 to 35° was achieved for applied electric fields in the range of 1 to 2.5  $\text{V } \mu\text{m}^{-1}$  at 26 GHz.

An exploratory experiment was made to test the BST-based LTCC in a multilayer configuration and assess its compatibility with commercial tapes. Due to the interest in integrating other devices into LTCC multilayer structures (see Fig. 2), exploratory experiments were carried out testing the compatibility of the BST-based LTCC with piezoelectric, ferrite and dielectric resonator ceramics. The results, although promising, pointed to the need for further development to optimize processing parameters.

In summary, the study led to the development of a successful LTCC material based upon MgO-modified BST and its exploitation in a novel microwave device.

## References

- Abe Y, Gunji T, Kimata Y, Kuramata M, Kasgöz A & Misono T (1990) Preparation of polymetalloxanes as a precursor for oxide ceramics. *J Non-Cryst Solids* 121: 21-25.
- Acikel B, Liu Y, Nagra AS, Taylor TR, Hansen PJ, Speck JS & York RA (2001) Phase shifter using (Ba,Sr)TiO<sub>3</sub> thin films on sapphire and glass substrates. *IEEE MTT-S Dig* 2: 1191-1194.
- Ayguavives T, Tombak A, Maria JP, Stauff GT, Ragaglia C, Roeder J, Mortazawi A & Kingon AI (2000) Physical properties of (Ba,Sr)TiO<sub>3</sub> thin films used for integrated capacitors in microwave applications. *Proc. the 12th IEEE International Symposium on Applications of Ferroelectrics (ISAF 2000)*, 21 July-2 Aug, Honolulu, HI USA, 1: 365-368.
- Babbitt R, Kosciwa T, Drach W & Didomenico (1995) Ferroelectric phase shifters and their performance in microwave phased array antennas. *Integrated Ferroelectr* 8: 65-76.
- Bailey A, Foley W, Hageman M, Murray C, Piloto A, Sparks K & Zaki K (1997) Miniature LTCC filters for digital receivers. *IEEE MMT-S Dig* 2: 999-1002.
- Barnwell P & O'Neill MP (1997) Enabling ceramic circuit technologies for wireless microelectronics packaging. *1997 Wireless Communications Conference*, Aug 11-13, Boulder, Colorado, USA, 156-161.
- Brinker CJ & Scherer GW (1990) *Sol-gel Science: the physics and chemistry of sol-gel processing*. Academic Press, London, UK, p 839-870.
- Cahn RW, Haasen P and Kramer EJ (1996) *Materials Science and Technology*, Vol. 17A, in *Processing of Ceramics* (Vol. Ed. Brook, R.J.), VCH Verlagsgesellschaft mbh. Cambridge Press, Chap 7: 242.
- Cho CW, Cho YS, Yeo JG, Kim J & Paik U (2003) Effect of PVB on the gelation behaviour of BaTiO<sub>3</sub>-based dielectric particles and glass suspension. *J Eur Ceram Soc* 23: 2315-2322.
- De Flaviis F, Chang D, Alexopoulos NG & Stafsudd OM (1996) High purity ferroelectric materials by sol-gel process for microwave applications, *IEEE MTT-S Dig* 1: 99-102.
- De Flaviis F, Alexopoulos NG & Stafsudd O (1997) Planar microwave integrated phase-shifter design with high purity ferroelectric material. *IEEE Trans Microwave Theory Tech* 45(6): 963-969.
- De Vries JWC, Jedeloo P & Porath R (1996) Co-fired piezoelectric multilayer transformers. *ISAF'96, Proc. the Tenth IEEE International Symposium on Applications of Ferroelectric*, Aug 18-21, East Brunswick, NJ, USA, 1: 173-176.

- Erker EG, Nagra AS, Liu Y, Periaswamy P, Taylor TR, Speck J, York RA (2000) Monolithic Ka-band phase shifter using voltage tunable BaSrTiO<sub>3</sub> parallel plate capacitors. *IEEE Microwave Guided Wave Lett* 10(1): 10-12.
- Gevorgian SS & Kollberg EL (2001) Do we really need ferroelectrics in paraelectric phase only in electrically controlled microwave devices? *IEEE trans. Microwave Theory Tech* 49(11): 2117-2124.
- Grigas J (1996) *Microwave Dielectric Spectroscopy of Ferroelectrics and Related Materials, Ferroelectricity and Related Phenomena*, vol. 9, Gordon and Breach Publishers, Amsterdam.
- Herner SB, Selmi FA, Varadan VV & Varadan VK (1993) The effect of various dopants on the dielectric properties of barium strontium titanate. *Mater Lett* 15: 317-324.
- Ho IC (1994) Semiconducting barium titanate ceramics prepared by boron-containing liquid-phase sintering. *J Am Ceram Soc* 77(3): 829-832.
- Howatt G, Breckenridge RG and Brownlow JM (1947) Fabrication of thin ceramic sheets for capacitors. *J Am Ceram Soc* 30(8): 237-242.
- Hu T, Jantunen H & Leppävuori S (2003) Co-firing of ferroelectric tapes and commercial LTCCs for tunable microwave components. *European Microwave Conference*, October 6-10, Munich, Germany.
- Hu T, Uusimäki A, Jantunen H, Leppävuori S, Soponmanee K & Sirisoonthorn S (2003) Optimization of MgTiO<sub>3</sub>-CaTiO<sub>3</sub> based LTCC tapes containing B<sub>2</sub>O<sub>3</sub> for use in microwave applications. *Ceramics International*, accepted.
- Ishizaki T, Yamada T & Miyake H (2000) A first practical model of very small and low insertion loss laminated duplexer using LTCC suitable for W-CDMA portable telephones. *IEEE MMT-S Dig 1*: 187-190.
- Jang SI & Jang HM (1998) Structure and electrical properties of boron-added (Ba,Sr)TiO<sub>3</sub> thin films fabricated by the sol-gel method. *Thin Solid Films* 330: 89-95.
- Jantunen H (2001) A novel low temperature co-firing ceramic (LTCC) material for telecommunication devices. *Acta Univ Oul C163*.
- Jantunen H, Leppävuori S, Turunen A & Uusimäki A (2001) Multilayer resonators and a bandpass filter fabricated from a novel Low Temperature Co-fired Ceramic. *J Electric Mater* 31(3): 191-195.
- Joshi SC, Lam YC, Boe FYC & Tok AIY (2002) Power law fluids and Bingham plastics flow models for ceramic tape casting. *J Mater Proc Tech* 120: 215-225.
- Kageyama K, Saito K, Murase H, Utaki H & Yamamoto T (2001) Tunable active filters having multilayer structure using LTCC. *IEEE Trans. Microwave Theory Tech* 49: 2421-2424.
- Kingery WD, Bowen, HK; Uhlmann DR (1976) *Introduction to ceramics*. New York, Wiley.
- Kittilä M, Hagberg J, Pudas M & Leppävuori S (2003) Printing with gravure methods in electronics. *14th European Microelectronics and Packaging Conference & Exhibition*, June 23-25, Friedrichshafen, Germany.
- Kulke R, Simon W, Lauer A, Rittweger M, Waldow P, Stringfellow S, Powell R, Harrison M & Bertinet JP (2001) Investigation of ring-resonators on multilayer LTCC. *Workshop on Ceramic Interconnect Technologies, International Microwave Symposium (IMS 2001)*, Phoenix, 21st May 2001.
- Lancaster MJ, Powell J & Porch A (1998) Thin-film ferroelectric microwave devices. *Supercond Sci Technol* 11: 1323-1334.
- Lee BI & Pope EJA (1994) *Chemical Processing of Ceramics*. Marcel Dekker, Inc. 270 Madison Avenue, New York.

- Levin EG, Robbins CR & McMurdie HF (1964) Phase Diagrams for Ceramics. Ed. By Reser MK, The American Ceramic Society Inc., Ohio, USA. p 91.
- Miranda FA, Mueller CH, Cabbage CD, Bhasin KB (1995) HTS/Ferroelectric thin films for tunable microwave components. IEEE Trans. Appl Supercond 5(2):3191-3194.
- Mistler RE & Twinaer ER (2000) Tape Casting: theory and practice. The American Ceramic Society, Westerville, Ohio, p 1-6, 8-14, 240.
- Moulson AJ & Herbert JM (2003) Electroceramics: Materials, Properties, Applications. Second Edition, John Wiley & Sons Inc., England.
- Ngo E, Joshi PC, Cole MW & Hubbard CW (2001) Electrophoretic deposition of pure and MgO-modified  $Ba_{0.6}Sr_{0.4}TiO_3$  thick films for tunable microwave devices. Appl Phys Lett 79(2): 248-250.
- Outzourhit A, Trefny JU, Kito T, Yarar B, Naziripour A & Hermann AM (1995) Fabrication and characterization of  $Ba_{1-x}Sr_xTiO_3$  tunable thin film capacitors. Thin Solid Films 259: 218-224.
- Padmini P, Taylor TR, Lefevre MJ, Nagra AS, York RA & Speck JS (1999) Realization of high tunability barium strontium titanate thin films by RF magnetron sputtering. Appl Phys Lett 75: 3186-3188.
- Ritter JJ (1986) Alkoxide precursor synthesis and characterization of phases in the barium-titanium oxide system. J Am Ceram Soc 69(2): 155-161.
- Rhim SM, Hong S, Bak H, Kim OK (2000) Effects of  $B_2O_3$  addition on the dielectric and ferroelectric properties of  $Ba_{0.7}Sr_{0.3}TiO_3$  Ceramics. J Am Ceram Soc 83(5): 1145-1148.
- Rhim SM, Bak H, Hong S & Kim OK (2000) Effects of heating rate on the sintering behavior and the dielectric properties of  $Ba_{0.7}Sr_{0.3}TiO_3$  ceramics prepared by boron-containing liquid-phase sintering. J Am Ceram Soc 83(12): 3009-3013.
- Richerson DW (1992) Modern Ceramic Engineering: properties, processing, and use in design. Second edition, Marcel Dekker, Inc., New York, p 519-590.
- Rupprecht G & Bell PO (1962) Microwave losses in strontium titanate above the phase transition. Phys Rev 125: 1915-1920.
- Scrantom CQ & Lawson JC (1999) LTCC technology: Where we are and where we're going-II, 1999 IEEE MTT-S Dig 193-200.
- Sengupta *et al.* (1995) Ceramic ferroelectric composite material: BST-MgO. U.S. Patent 5,427,988.
- Sengupta LC & Sengupta S (1999) Breakthrough advances in low loss, tunable dielectric materials. Mater Res Innovations 2: 278-282.
- Smolenskii GA & Isupov VA (1954) Zhurnal Tekhnicheskoi Fiziki 24, 1375.
- Su B & Button TW (2001) Interactions between barium strontium titanate (BST) thick films and alumina substrates. J Eur Ceram Soc 21: 2777-2781.
- Su B & Button TW (2004) Microstructure and dielectric properties of Mg-doped barium strontium titanate ceramics. J App Phy 95(3): 1382-1385.
- Syamaprasad U, Galgali RK & Mohanty BC (1988) Dielectric properties of the  $Ba_{1-x}Sr_xTiO_3$  system. Mater Lett 7: 197-200.
- Tombak A, Ayguavives FT, Maria JP (2000) Low voltage tunable barium strontium titanate thin film capacitors for RF and microwave applications. IEEE MTT-S Dig 1345-1348.
- Tombak A, Ayguavives FT, Maria J, Stauf GT, Kingon AI & Mortazawi A (2001) Tunable RF filters using thin film barium strontium titanate based capacitors, 2001 IEEE MTT-S Dig 1453-1456.

- Tummala RR (1991) Ceramic and glass-ceramic packaging in the 1990s. *J Am Ceram Soc* 74(5): 895-908.
- Vendik OG & Zubko SP (2000) Ferroelectric phase transition and maximum dielectric permittivity of displacement type ferroelectrics ( $\text{Ba}_x\text{Sr}_{1-x}\text{TiO}_3$ ). *J Appl Phys* 88(9): 5343-5350.
- Vendik IB, Vendik OG & Kollberg EL (2000) Commutation quality factor of two-state switchable devices. *IEEE Trans. Microwave Theory Tech* 48: 802-808.
- Wang FY (1976) *Treatise on Material Science and Technology*. Vol. 9, Ceramic Fabrication Processes. New York: Academic Press.
- Wang SF, Huebner W & Dougherty JP (1994) Correlation of wettability and interfacial reaction to the densification and dielectric properties of fluxed-  $\text{BaTiO}_3$ . *Proceedings of the Ninth IEEE International Symposium on Applications of Ferroelectrics*, Aug 7-10, University Park, PA, USA, 581-584.
- Yao K, Zhu W & Yao X (1998) Development of Ba-Ti-B glass-ceramic thick-film capacitors by sol-gel technology. *IEEE Trans, Components, Packaging, and Manufacturing Technol, Part C* 21(1): 21-25.
- Zimmermann F, Voigts M, Weil C, Jakoby R, Wang P, Menesklou W & Ivers-Tiffée E (2001) Investigation of barium strontium titanate thick films for tunable phase shifters. *J Eur Ceram Soc* 21: 2019-2023.